Highly regenerative species-specific genes improve age-associated features in the adult *Drosophila* midgut

Hiroki Nagai[1], Yuya Adachi[1], Tenki Nakasugi[1], Ema Takigawa[1], Junichiro Ui[1], Takashi Makino[2], Masayuki Miura[1], and Yu-ichiro Nakajima[1] *

1. Graduate School of Pharmaceutical Sciences, The University of Tokyo

2. Graduate School of Life Science, Tohoku University

*Author for correspondence e-mail: nakaji97@g.ecc.u-tokyo.ac.jp

Tel: +81-3-5841-4863

Text: 35580 characters

Figures: 7

Supporting information: Supplemental figures S1-S4, Supplemental tables S1-S2, Supplemental texts S1

Abstract

Background

The remarkable regenerative abilities observed in planarians and cnidarians are closely linked to the active proliferation of adult stem cells and the precise differentiation of their progeny, both of which typically deteriorate during aging in low regenerative animals. While regeneration-specific genes conserved in highly regenerative organisms may confer regenerative abilities and long-term maintenance of tissue homeostasis, it remains unclear whether introducing these regenerative genes into low regenerative animals can improve their regeneration and aging processes.

Results

Here we ectopically express high regenerative species-specific JmjC domain-encoding genes (HRJDs) in *Drosophila*, a widely used low regenerative model organism. Surprisingly, HRJD expression impedes tissue regeneration in the developing wing disc but extends organismal lifespan when expressed in the intestinal stem cell lineages of the adult midgut under non-regenerative conditions. Notably, HRJDs enhance the proliferative activity of intestinal stem cells while maintaining their differentiation fidelity, ameliorating age-related decline in gut barrier functions.

Conclusions

These findings together suggest that the introduction of highly regenerative species-specific genes can improve stem cell functions and promote a healthy lifespan when expressed in aging animals.

Keywords

Synthetic biology, aging, healthy lifespan, regeneration, *Drosophila*, intestinal stem cells

INTRODUCTION

Regeneration, an intricate process that rebuilds lost body parts, is a widespread phenomenon among metazoans, but the capacity for regeneration displays significant variation across different groups and species [1–5]. While certain animals like planarians and hydras possess the remarkable ability to regenerate their entire body from a small fragment, other groups with more complex body structures, such as mammals and insects, exhibit a diminished regenerative potential and can only regenerate specific tissues and/or organs to a limited extent. Furthermore, regenerative capacity often declines with aging in most species with limited regeneration abilities [2], resulting in increased susceptibility to organismal death upon injury. In contrast, animals that can achieve whole body regeneration, along with developmental reversion observed in the jellyfish *Turritopsis*, exhibit potential immortality [2, 5, 6]. Understanding the mechanisms underlying high regenerative ability and their relationship with aging represents a fundamental challenge in the field of developmental biology and gerontology with implications for regenerative medicine.

Several cellular and molecular factors have been identified as determinants of regeneration capacity. Highly regenerative animals such as planarians and cnidarian polyps rely on pluripotent adult stem cells, called neoblasts and interstitial cells (i-cells),

65 respectively [2–5, 7]. These stem cells migrate to the injury sites and contribute to the
66 formation of a blastema, an undifferentiated cellular mass, enabling the restoration of
67 amputated body structures. Some vertebrates like salamanders and fish, which do not
68 possess adult pluripotent stem cells, can regenerate organs after injury by recruiting
69 blastema cells through dedifferentiation and/or the activation of quiescent lineage-
70 restricted stem cells [1, 2, 4, 5, 8]. At the molecular level, the evolutionary conserved
71 WNT signaling pathway promotes a wide range of regenerative events across species,
72 including blastema formation in newts and *Hydra* [1–5, 8].

73 In contrast to the conserved regulators of regeneration, several genes are
74 specific to highly regenerative animal groups and species: for instance, the newt gene
75 *Prod1* regulates re-patterning during limb regeneration [9, 10], and viropana family
76 (*viropana 1-5*) is up-regulated during lens regeneration [11, 12]. These species/group-
77 specific genes might explain differences in regeneration capacity between species.
78 Remarkably, ectopic expression of *viropana 1-5* can enhance regeneration of the
79 primordium of *Drosophila* eyes that maintain regenerative capacity during development
80 [12]. This finding raises the possibility that heterologous induction of regenerative genes
81 may accelerate tissue regeneration, at least in developing animals, and potentially provide
82 a cue for developing novel regenerative therapies. However, it remains unknown whether
83 heterologously-induced regenerative genes can improve regenerative and/or aging
84 processes even when induced in post-developmental mature adults.

85 Notably, given that basal metazoans such as Porifera, Ctenophore, Placozoa,
86 and Cnidaria all exhibit robust regenerative abilities, it is conceivable that a common

87 ancestor of all metazoans once possessed a high regenerative potential and independently
88 lost genes related to high regenerative capacity in multiple phyla. Building upon this
89 hypothesis, bioinformatics analysis has identified genes that are common among species
90 with high regenerative abilities and absent in species with limited regenerative capacities
91 (Fig. 1A) [13]. The highly regenerative species-specific JmjC domain-encoding genes
92 (HRJDs) are a group of such genes (with typically two or three orthologs per species)
93 characterized by their JmjC domain (Fig. 1A), yet their molecular functions remain
94 unknown. Given their potential influence on the regenerative process, HRJDs may
95 contribute to the high regeneration potential of highly regenerative animals. With this in
96 mind, a question arises: what would happen if a low regenerative species, which has lost
97 HRJDs, were to acquire them again? By ectopically expressing HRJDs in low
98 regenerative animal models, we can investigate their impacts on regeneration as well as
99 on aging processes, providing insight into the role of HRJDs.

100 Here we express HRJDs in the fruit fly *Drosophila melanogaster* and evaluate
101 their impact *in vivo*, especially by focusing on two epithelial tissues: developing wing
102 discs and post-developmental adult midguts, both of which exhibit regeneration potential
103 and can replenish damaged epithelial cells. In contrast to the predicted contribution of
104 HRJDs in regeneration as observed in planarian, ectopic HRJD induction impedes
105 regenerative responses and decreases organismal survival upon injury in *Drosophila*.
106 Surprisingly, however, HRJD expression in the stem/progenitor population of the adult
107 midguts extends organismal lifespan under the non-regenerative condition. Further
108 investigations reveal that HRJDs enhance the proliferative activity of intestinal stem cells

while keeping their differentiation fidelity in aged guts, ameliorating age-related decline in gut barrier functions. These findings provide evidence that genes specific to highly-regenerative animals can improve stem cell function as well as increase healthy lifespan upon heterologous expression in aging animals.

RESULTS

Planarian HRJDs expression do not affect gross morphology of fly adults

Planarians are one of the most highly regenerative animals; they are capable of regenerating most body parts upon amputation and can even reconstruct their whole body from fragments [1–4, 8, 14]. Previous work has identified two HRJD orthologs *HRJDa* and *HRJDb* from two planarian species, *Dugesia japonica* and *Schmidtea mediterranea*, where both HRJDs contain only the JmjC domain and the EF hand motif (Fig. 1B) [13]. In functional assays using RNAi-mediated knockdown in *D. japonica*, these two HRJDs affect viability of organisms after amputation [13], suggesting that planarian HRJDs are associated with regeneration processes. We thus utilized these functional HRJDs in *D. japonica* as representatives for the following studies and hereafter simply named them as HRJDa and HRJDb.

To examine potential benefits and/or disadvantages of acquiring HRJDs, we then ectopically expressed HRJDs in *Drosophila melanogaster*, which has lost HRJD genes during evolution (Fig. 1A), using the Gal4/UAS system (Fig. S1) [15]. We first introduced HRJDs in the whole body throughout development with the ubiquitous driver *Act5C-Gal4* (Fig. 1C, *Act5C-Gal4>UAS-HRJDa/b*). The whole body expression of

131 HRJDs neither caused developmental lethality nor changed the body weight of mature
132 adults compared with the *Act5C-Gal4>UAS-GFP* control (Fig. 1D and 1E). We further
133 assessed the gross morphology of adult wings and eyes under the ubiquitous expression
134 of HRJDs. The wing size was not altered by HRJD expression (Fig. 1F and 1G). Similarly,
135 *Act5C-Gal4>UAS-HRJDa/b* flies did not change the size of adult compound eyes (Fig.
136 1H and 1I). These results indicate that HRJD expression does not disturb gross
137 morphology of adult flies under homeostatic conditions, likely due to minimal impacts
138 on developmental processes.
139
140 **HRJD expression hampers tissue regeneration in the developing wing disc**
141 Given that HRJDs are conserved only among highly regenerative animals, their primary
142 functions may be related to regeneration processes. Indeed, both planarian HRJDa and
143 HRJDb function in whole-body regeneration while their relative contribution is likely
144 context-dependent: HRJDa is indispensable for the regeneration of amputated heads
145 while HRJDb promotes organismal survival after two consecutive amputations [13]. To
146 test whether heterologously-induced HRJDs can enhance regenerative responses in
147 *Drosophila*, we examined their impacts on regeneration after ablation of the developing
148 wing imaginal disc. The *Drosophila* larval imaginal discs, including wing discs, which
149 are composed of columnar epithelial cells, exhibit regenerative capacity and restore
150 morphology even after massive cell death [16, 17] (Fig. 2A and 2B). We utilized the
151 genetic ablation system in which transient overexpression of *eiger*, a *Drosophil*a TNF
152 ligand, induces apoptosis in the wing pouch region [17, 18]. In this tissue ablation system,

153 the temperature-sensitive form of the Gal4 repressor Gal80 (*tub-Gal80^{ts}*) allows transient
154 tissue ablation under the control of a wing pouch driver *rn-Gal4*. To circumvent the
155 temporal expression associated with the Gal4/Gal80^{ts} system, we further introduced an
156 additional binary expression system: the QF/QUAS system for HRJD induction (Fig. 2A)
157 [19, 20]. When expressing HRJDs in the wing pouch with the *WP-QF* driver during the
158 entire process of recovery, we found that *WP-QF>QUAS-HRJDs* flies exhibit severe
159 defects compared to controls (Fig. 2C). Immunostaining of a mitotic marker, phospho-
160 histone H3 (PH3), revealed that HRJD expression resulted in a slight but not statistically
161 significant decrease in regenerative proliferation in the wing pouch, implying the
162 possibility of insufficient damaged cell replenishment (Fig. 2D and 2E). Importantly,
163 HRJD induction in the wing disc affected neither the development of the adult wing nor
164 proliferation in wing discs under homeostatic condition (Fig. 2F-2I). These results
165 suggest that HRJD expression does not facilitate regeneration in the developing wing disc
166 epithelium.
167
168 **HRJD expression compromises regeneration in the adult midgut**
169 Most highly regenerative animals exhibit regeneration potential in mature adult stages
170 [2–4, 8], and thus one possibility is that HRJDs stimulate regenerative responses only in
171 adults, where tissue-resident stem cells play an important role in homeostasis and
172 regeneration. We thus tested the impact of HRJD expression on the regenerative capacity
173 of the *Drosophila* adult midgut. In the adult midgut, intestinal stem cells (ISCs) self-
174 renew ISCs themselves and also generate differentiating progenitor cells called

175 enteroblasts (EBs) and enteroendocrine progenitors (EEPs), which eventually
176 differentiate into absorptive enterocytes (ECs) and secretory enteroendocrine cells (EEs),
177 respectively (Fig. 3A) [21–24]. The adult midgut activates proliferation of ISCs in
178 response to orally-treated harmful chemicals such as paraquat and dextran sulfate sodium
179 (DSS), a regenerative response that is essential for organismal survival [21, 25–28]. We
180 thus expressed HRJDs in ISCs and EBs using the *esg-Gal4* (*esg-Gal4>UAS-HRJDa/b*)
181 driver and tested survival against paraquat/DSS damage. Similar to the wing regeneration
182 assay, continuous expression of HRJDs via *esg-Gal4* significantly impaired organismal
183 survival upon the chemical challenges, with a stronger effect for HRJDa (Fig. S2A and
184 S2B). Survival under control feeding (5% sucrose) was also slightly decreased by HRJD
185 expression, albeit not to a statistically significant degree (Fig. S2C). We further examined
186 ISC proliferation after paraquat feeding by counting the number of cells marked with a
187 mitotic marker, anti-PH3 staining, and found that induction of HRJDa significantly
188 suppressed ISC division (Fig. S2D), which is consistent with the stronger decline in
189 survival rate. Concordant with the wing ablation experiments, these results suggest that
190 continuous HRJD expression causes detrimental effects to regenerative capacity.

191 Because the *esg-Gal4* driver is active not only in adult ISCs/EBs but also in the
192 proliferative adult midgut progenitors in the larval midguts and larval imaginal discs [29,
193 30], continuous HRJD expression may cause internal organ defects associated with
194 development. To temporally restrict HRJD expression to the adult stage, we next set up
195 an experiment where HRJD expression starts only in adults after eclosion from pupa by
196 combining *esg-Gal4* with *tub-Gal80^{ts}* (*esg-Gal4^{ts}>UAS-HRJDa/b*) (Fig. 3B); however,

197 neither HRJDa nor HRJDb improved organismal survival upon paraquat/DSS feeding
198 (Fig. 3C and 3D). Instead, HRJDa expression caused a slight but significant decrease in
199 survival rate compared to controls (*esg-Gal4^{ts}>UAS-GFP*). HRJDb expression similarly
200 resulted in decreased survival at late phase (Day 4 and Day 5 in paraquat feeding, Day 5
201 and Day 6 in DSS feeding) , though not to a statistically significant degree (Fig. 3C and
202 3D). Survival under control feeding (5% sucrose) was comparable between *esg-*
203 *Gal4^{ts}>UAS-GFP* and *esg-Gal4^{ts}>UAS-HRJDa/b* (Fig. 3E), suggesting that the impaired
204 survival of *esg-Gal4^{ts}>UAS-HRJDs* is specific to regenerative contexts. We also found
205 that, after paraquat feeding, mitotic cell numbers in HRJD expressing flies decreased
206 slightly (Fig. 3F and 3G), suggesting the possibility of impaired regeneration. These
207 results indicate that post-developmental expression of HRJDs does not enhance intestinal
208 regeneration in adult flies.
209
210 **Post-developmental HRJD expression in ISC lineages extends organismal lifespan**
211 Highly-regenerative animals are often resistant to organismal aging and have long
212 lifespan; some species like the jellyfish *Turritopsis* even revert their early developmental
213 stages under harsh environments and are considered to be potentially immortal [2, 6].
214 Although heterologous expression of HRJDs does not augment tissue regeneration in
215 either developing or adult *Drosophila* tissues, we further investigated whether HRJDs
216 influence organismal lifespan under homeostatic conditions in which no experimental
217 injuries are applied to fly adults. We observed that post-developmental HRJD expression
218 in adult ISCs/EBs (*esg-Gal4^{ts}>UAS-HRJDa/b*) significantly extended organismal

219 lifespan both in females (Fig. 4A) and males (Fig. 4B). In contrast, continuous HRJD
220 expression in the whole body (*Act5C-Gal4>UAS-HRJDa/b*) shortened males' lifespan
221 (Fig. 4C and 4D). Moreover, HRJD expression in differentiated ECs (*NP1-Gal4>UAS-*
222 *HRJDa/b*) also negatively impacted female lifespan, likely due to developmental
223 abnormalities since EC-specific HRJD expression in the adult stage did not decrease
224 survival (Fig. S3A-S3D). These results suggest that spatio-temporally regulated induction
225 of HRJDs in adult ISCs/EBs can be beneficial for adult flies under homeostatic conditions.
226 Further investigation revealed the distinct impacts of HRJDa and HRJDb on
227 organismal lifespan: while continuous expression of HRJDa via *esg-Gal4 (esg-*
228 *Gal4>UAS-HRJDa)* shortened lifespans for both males and females, *esg-Gal4>UAS-*
229 *HRJDb* prolonged female lifespans but shortened male lifespans (Fig. S3E and S3F). The
230 ortholog-dependent phenotypic differences were also reported in planarian regeneration
231 [13]. To address the mechanisms of lifespan extension associated with post-
232 developmental HRJD expression in ISCs/EBs, we focused on *esg-Gal4^{ts}>UAS-HRJDs*
233 midguts in the following experiments.
234
235 **HRJD expression improves barrier function in the aged intestine**
236 Age-related mortality accompanies intestinal barrier dysfunction and disruption of cell-
237 cell junction in the gut epithelium across species [31–34]. Given that aging phenotypes
238 are more severe in female flies than male flies [35], we first tested barrier function of the
239 *esg-Gal4^{ts}>UAS-HRJDa/b* female midgut using the Smurf assay, in which orally-
240 administered blue dye spreads throughout the entire body when the intestinal barrier is

241 disrupted (Smurf+, Fig. 5A) [31, 35]. Consistent with lifespan extension, post-
242 developmental HRJD expression in ISCs/EBs significantly decreased the ratio of Smurf+
243 adults at 30-days old, a time point where age-related organismal death starts (Fig. 4A and
244 5A), suggesting that barrier function is maintained in aged flies that express HRJDs in
245 ISCs/EBs. We further assessed the localization of septate junction markers (Dlg, Tsp2A,
246 Mesh, Ssk), which diffuse in cytoplasm in the aged midgut [33, 36–38]. The diffusion of
247 the Dlg protein in aged midguts was significantly suppressed in *esg-Gal4*^{ts}*>UAS-*
248 *HRJDa/b* midguts (Fig. 5B and 5C). Similarly, peripheral localization of Tsp2A, Mesh,
249 and Ssk proteins was also maintained in *esg-Gal4*^{ts}*>UAS-HRJDa/b* midguts compared
250 with control (*esg-Gal4*^{ts}*>UAS-GFP*) midguts (Fig. 5D-5I). Given that HRJDs in
251 ISCs/EBs affect localization of junctional components in ECs, we next tested if HRJDs
252 non-autonomously affect junctional integrity. To this end, we performed a mosaic
253 experiment where HRJDs were clonally induced using the esgFLPout system [26]. Clonal
254 induction of HRJDs improved junctional localization of Ssk both inside and outside the
255 clones (Fig. S4A and S4B), supporting the conclusion that HRJDs' effect is non-cell
256 autonomous. We then examined JNK activation in ECs, which is associated with barrier
257 dysfunction in the aged intestine [27, 36]. HRJD expression in ISCs/EBs significantly
258 repressed transcription of *puckered* (*puc*), a downstream target of JNK signaling in the
259 whole midgut (Fig. 5J), and indeed the intensity of *puc-lacZ* reporter decreased in ECs
260 upon HRJD induction (Fig. 5K and 5L). HRJD expression in ISCs/EBs thus suppresses
261 JNK signaling in ECs in the aged midgut, which is mediated by either a non-autonomous
262 function of HRJDs or residual HRJD proteins in newly differentiated ECs. These results

263 indicate that HRJD expression in adult ISCs/EBs contributes to the prolonged
264 maintenance of the junctional integrity as well as gut barrier function in the aged intestine.
265

266 **HRJD expression attenuates mis-differentiation of stem cell lineage in the aged**
267 **intestine**

268 In addition to the intestinal barrier dysfunction, aberrant activation of ISC mitosis and
269 accumulation of mis-differentiated ISC progenies are also common age-related
270 phenotypes in the *Drosophila* adult midgut [27, 31, 33, 39]. In 30-days old control
271 midguts, *esg-Gal4*^{ts}*>UAS-GFP*$^{+}$ cells exhibited hallmarks of age-related mis-
272 differentiation into ECs such as increased ploidy and enlarged nuclear size (Fig. 6A) [27].
273 By contrast, we found that HRJD expression in adult ISCs/EBs suppressed these mis-
274 differentiation phenotypes (Fig. 6A and 6B), which are consistent with the amelioration
275 of age-related barrier dysfunction in *esg-Gal4*^{ts}*>UAS-HRJDa/b* midguts. Surprisingly,
276 however, *esg-Gal4*^{ts}*>UAS-HRJDa/b* did not suppress age-related increase in ISC
277 proliferation, but rather enhanced it in 30-day old midguts (Fig. 6C and 6D). The
278 enhancement of ISC proliferation was specific to the aged intestine since *esg-*
279 *Gal4*^{ts}*>UAS-HRJDs* did not affect PH3^{+} cell number in 10-day-old young midguts (Fig.
280 S4E). These results raised the possibility that HRJD expression augments the mitotic
281 activity of stem cells while maintaining their differentiation fidelity during aging.

282 To test this hypothesis, we first measured the expression of cell type markers
283 (*Delta* for ISCs, *nub* for ECs, and *pros* for EEs) by RT-qPCR of whole midguts. Both *nub*
284 and *pros* are negatively regulated by Esg [40, 41], and accumulation of *esg*$^{+}$ mis-

285 differentiated cells accompanies the down-regulation of EC-related genes in aged midguts
286 [27]. Consistent with enhanced ISC proliferation, *esg-Gal4^{ts}>UAS-HRJDa* significantly
287 up-regulated *Delta* (*Dl*) expression in 30-day old midguts (Fig. 6E). More importantly,
288 *esg-Gal4^{ts}>UAS-HRJDa* also up-regulated *nub* and *pros*, which supports our hypothesis
289 that HRJDs improve proper differentiation of ISC progenies. In *esg-Gal4^{ts}>UAS-HRJDb*,
290 only *Dl*, but not *nub* and *pros*, was up-regulated when whole midguts were used as sample
291 (Fig. 6E). Next, we focused on the posterior midgut where both HRJDa and HRJDb
292 prevent mis-differentiation of EBs (Fig. 6A), and examined cell type composition using
293 the combination of markers *esg^{ts}>GFP* (ISC/EB), *Dl-lacZ* (ISC/EEP), and anti-Pros
294 (EEP/EE). Consistent with the prevention of EB mis-differentiation, *esg^{ts}*-mediated
295 HRJD expression decreased EBs (esg^{+}Dl^{-}Pros^{-}) and increased polyploid ECs
296 (esg^{-}Dl^{-}Pros^{-}) compared to the control midgut (Fig. 6F and 6G). These results indicate
297 that HRJDs improve differentiation fidelity in ISC lineage.

298 To address the potential mechanism of HRJD-dependent maintenance of ISC
299 functions, we focused on the JAK-STAT pathway since its activation promotes both ISC
300 proliferation and differentiation into ECs [26, 42, 43]. In young mature midguts, STAT
301 activity is largely restricted to *esg*$^{+}$ ISCs/EBs [26, 42, 44]. In aged midguts, however, a
302 subset of polyploid cells exhibited weak signal of the STAT reporter *10×STAT-GFP*,
303 likely due to the accumulation of mis-differentiated EBs (Fig. 6H). Notably, HRJD
304 induction canceled such ectopic STAT activation in polyploid cells and rather enhanced
305 STAT activity in diploid ISCs/EBs (Fig. 6H and 6I), which is consistent with our
306 observations that HRJDs boost ISC functions during aging. These results suggest that

307 HRJD expression accelerates the generation of differentiated ECs via JAK-STAT
308 activation. In the healthy homeostatic intestine, ISC division and subsequent
309 differentiation into ECs is coupled with the loss of old ECs [45, 46]. Interestingly, we
310 found that *esg*-lineage clones that express HRJDs rapidly replaced pre-existing cells by
311 generating polyploid ECs (Fig. S4A, S4C, and S4D). In addition, more cells exhibited
312 cleaved Dcp1, an apoptotic marker, in 30-day old esg^{ts} >*HRJDs* midguts (Fig. S4F and
313 S4G), implying that HRJD induction promotes turnover of midgut epithelial cells.
314 Collectively, our data show that post-developmental expression of HRJDs improves stem
315 cell functions in the aged intestine.
316

317 **DISCUSSION**

318 In this study, we demonstrate that post-developmental expression of planarian HRJD
319 genes in the *Drosophila* adult ISCs/EBs can suppress age-related intestinal dysfunctions
320 and extend organismal lifespan, while their continuous expression throughout the entire
321 developmental process hampers regenerative responses and principally shortens lifespan.
322 Notably, HRJDs in adult ISCs/EBs boost the age-related increase of ISC proliferation but
323 do not cause age-related mis-differentiation of ISC progenies (Fig. 7). These HRJD-
324 mediated outcomes are distinct from those mediated by typical anti-aging manipulations
325 such as antibiotic treatment and metabolic intervention, which ameliorate both ISC over-
326 proliferation and mis-differentiation [24, 31, 47]. Therefore, heterologously induced
327 HRJDs create the neomorphic state in the aged intestine (Fig. 7). Given the age-related
328 increase of chronic cellular stresses [24, 27, 36, 47, 48], we speculate that the HRJD-

329 dependent ISC activation and their proper differentiation improve organismal fitness by
330 enabling active turnover of damaged intestinal cells.

331 Our investigation implies that the activation of the JAK-STAT pathway
332 underlies the HRJD-mediated enhancement of ISC functions. Surprisingly, however, the
333 expression of most mitogens including upstream ligands of JAK-STAT signaling (*upd1,*
334 *upd2, upd3*) were not up-regulated by HRJD induction (Fig. S4H), raising the possibility
335 that HRJDs activate STAT by modulating intracellular signaling factors. Such ligand-
336 independent STAT activation can be achieved via non-receptor type tyrosine kinases like
337 Src and Abl [49]. Given that the typical JmjC family proteins function as histone
338 demethylase or protein hydroxylase [50], HRJDs may epigenetically target these tyrosine
339 kinases. Notably, *Drosophila* Jarid2 (Jumonji, AT rich interactive domain 2) activates
340 EGFR signaling upon overexpression in ISCs/EBs without changing ligand expression
341 [51]. Our findings, together with these reports, suggest a cell-autonomous role of JmjC
342 family proteins in regulating proliferative signaling in stem cell lineages. Intriguingly,
343 Jarid2 expression in ISCs/EBs leads to ISC over-proliferation as well as barrier
344 dysfunction, resulting in reduced lifespan [51], which is the opposite adult phenotype of
345 HRJD expression in ISC lineages. Moreover, in contrast to the nuclear localization of
346 histone demethylase KDM8 [52, 53], the closest paralog of HRJDs, ectopically-induced
347 HRJDs localize in the cytoplasm but not in the nucleus both *in vitro* (S2 cells) and *in vivo*
348 (wing discs and adult midguts) (Fig. S1B-S1D). This is a common localization pattern of
349 JmjC-domain only proteins [53, 54] and implies that an unknown mechanism may operate
350 when HRJDs work as a potential histone demethylase. In the future, it will thus be critical

351 to examine the detailed molecular function of HRJDs to understand their impact on stem
352 cell lineages.

353 Although HRJDs have been identified as genes conserved between highly
354 regenerative animals [13], it is unclear whether HRJDs alone are sufficient to enhance
355 regenerative responses. Our investigations revealed that ectopic expression of HRJDs
356 failed to improve regeneration of developing wing discs and adult midguts in *Drosophila*
357 (Fig. 2 and 3), likely through the attenuation of regenerative growth. However, it should
358 be noted that we induced HRJDs before tissue injury and maintained their expression
359 during regeneration period. Given that *HRJDb* is up-regulated in the late phase of
360 planarian regeneration (3 days after amputation) [13], strict regulation of HRJD induction
361 might be important for their proper function as true regeneration regulators. On the other
362 hand, the expression level of *HRJDa* remains constant during planarian regeneration [13],
363 which is recapitulated in our experiments. Another possibility is that a high regeneration
364 ability can be achieved by cooperation between HRJDs and other unidentified genes that
365 have been lost during evolution, which should be addressed in future studies.

366 During the normal aging process in the *Drosophila* adult midgut, ISC over-
367 proliferation is closely linked with other aging phenotypes, and suppression of ISC
368 division can prevent the accumulation of mis-differentiated ISC progenies and extend
369 organismal lifespan [24, 36, 47, 48]. In contrast, HRJDs enhance age-related ISC
370 activation but can alleviate mis-differentiation and extend lifespan, suggesting that it is
371 not ISC activation itself but rather mis-differentiation of ISC progenies that principally
372 drives age-related mortality. Consistently, manipulation of mitotic spindle orientation,

373 which affects the cell fate of daughter cells [55–57], can extend organismal lifespan
374 without changing mitotic activity of ISCs [57]. Of note, in contrast to *Drosophila* ISCs
375 which over-proliferate in aged midguts, many adult stem cells decrease their activity and
376 abundance during aging both in *Drosophila* and mammals [24, 58, 59]. Future
377 investigations for mechanisms of HRJD-mediated stem cell rejuvenation will provide
378 clues to develop new anti-aging strategies.
379

380 **CONCLUSIONS**

381 In this study, we established a *Drosophila* model in which HRJDs are heterologously
382 expressed in specific tissue or cell type using binary expression systems, and
383 demonstrated that HRJDs can improve proliferative/differentiation capacity of ISCs in
384 the aged midgut. Although continuous HRJD expression in the wing disc and in the adult
385 midgut impairs tissue regeneration upon injury, restricted HRJD expression in post-
386 developmental adult ISCs/EBs enhances mitotic activity of ISCs as well as maintains
387 their differentiation fidelity in the aged flies, leading to the prevention of age-related
388 intestinal barrier dysfunction and the extension of organismal lifespan. Our HRJD-
389 expressing model will serve as a valuable resource to understand unprecedented
390 mechanisms of stem cell rejuvenation in the future.
391
392

393 **METHODS**

394 ***Drosophila* stocks**

395 All stocks were maintained on a standard diet containing 4% cornmeal, 6% baker's yeast
396 (Saf Yeast), 6% glucose (Wako, 049-31177), and 0.8% agar (Kishida chemical, 260-
397 01705) with 0.3% propionic acid (Tokyo Chemical Industry, P0500) and 0.05% nipagin
398 (Wako, 132-02635). Canton S was utilized as the wildtype strain. Transgenic fly lines
399 were obtained from the Bloomington Drosophila Stock Center (BDSC) and the Kyoto
400 Stock Center: *Act5C-Gal4* (BDSC 3954), *rn-Gal4, tub-Gal80ts, UAS-egr* (BDSC 51280),
401 *WP-QF2* [60], *tub-Gal80ts* (BDSC 7017, 7019), *esg-Gal4* (Kyoto 109126), *NP1-Gal4*
402 (Kyoto 112001), *UAS-GFP* (BDSC 1522), *M{3xP3-RFP.attP}ZH-86Fb* (Kyoto 130437),
403 *UAS-HRJDa* (this study), *UAS-HRJDb* (this study), *QUAS-HRJDa* (this study), *QUAS-*
404 *HRJDb* (this study), *UAS-FLAG-HRJDa* (this study), *UAS-FLAG-HRJDb* (this study),
405 *puc-lacZ* (BDSC 98329), *10×STAT-GFP* (BDSC 26198), *Dl-lacZ* (BDSC 11651). *esg-*
406 *Gal4, UAS-GFP, tub-Gal80ts; UAS-FLP, Act5C-FRT.CD2-Gal4* (esgFLPout) is a gift
407 from Irene Miguel-Aliaga. See **Table S1** for genotypes in each Figure. We used female
408 flies unless otherwise noted in the Figures.
409
410 ***Drosophila* genetics**
411 Experimental crosses that did not involve Gal80^{ts}-mediated inhibition of Gal4 were
412 performed at 25°C. When using Gal80^{ts}, experimental crosses were maintained at 18°C.
413 For genetic wing ablation experiments (Fig. 2), F1 larvae were raised at 18ºC until day 7,
414 incubated at 29ºC for the next 40 hr, and then maintained at 18ºC until the adult hatched
415 or dissection. For lifespan assays, midgut staining, and Smurf assays (Fig. 3-6); F1 adults
416 were transferred to 29°C three days after eclosion until the experiments. Midgut staining
417 and Smurf assays were performed after 7 or 27 days of 29°C incubation (young: Day 10
418 adults, old: Day 30 adults). For esgFLPout experiments, flies were maintained at 18°C
419 until 50 days, and 50-day old adults were transferred to 29°C and analyzed after 10 days
420 (final 60-day old).
421
422 **Generation of HRJD expressing lines**
423 To express HRJDs using the Gal4/UAS or the QF/QUAS system, we constructed a vector
424 containing *HRJDa* or *HRJDb* under the control of either the UAS sequence or QUAS
425 sequence. Namely we amplified HRJDa and HRJDb sequence from codon-optimized
426 synthesized DNAs (pUCIDT-HRJDa and pUCIDT-HRJDb, IDT, Supplementary texts
427 S1) for *DjHRJDa* (Genbank # LC408963) and *DjHRJDb* (Genbank # LC408964),

428 respectively. UAS-HRJDa and UAS-HRJDb were constructed by ligating HRJDa and
429 HRJDb into pUAST-attB (DGRC 1419), respectively (digested by EcoRI/NotI).
430 Similarly, QUAS-HRJDa and QUAS-HRJDb were constructed by ligating HRJDa and
431 HRJDb into pQUAS-WALIUM20 (DGRC 1474), respectively (digested by NheI/EcoRI).
432 To construct UAS-3xFLAG-HRJDs, we PCR-amplified the coding sequences of HRJDs
433 from pUCIDT-HRJDs by gene-specific primers with 3xFLAG tag at 5'-end of the
434 forward primers, and the amplicons were then ligated into a pUAST-attB vector digested
435 by EcoRI/NotI using In-Fusion HD Cloning Kit (Takara, 639649). The landing site for
436 each construct was {3xP3-RFP.attP}ZH-86Fb. Injection and selection were performed
437 by WellGenetics (Taiwan, R.O.C.). Please see also Table S2 and Supplementary texts S1
438 for primer sequences and HRJDs sequences.
439
440 **S2 cell culture**
441 *Drosophila* S2 cells were grown at 25°C in Schneider's *Drosophila* medium (GIBCO,
442 21720001) supplemented with 10% (v/v) heat-inactivated fetal bovine serum (FBS), 100
443 U/mL penicillin, and 100 μg/mL streptomycin (FUJIFILM Wako, 168–23191).
444
445 **S2 cell immunostaining**
446 To examine the expression pattern of HRJDs through immunostaining, 1×10^6 cells were
447 seeded in 6-well plates containing Schneider's *Drosophila* medium supplemented with
448 10% (v/v) heat-inactivated fetal bovine serum, 100 U/mL penicillin, and 100 μg/mL
449 streptomycin and were transfected with 800 ng of pAc5-3xFLAG-HRJDs using Effectene
450 Transfection Reagent (QIAGEN, 301427) following the manufacturer's protocol. To
451 prepare pAc5-3xFLAG-HRJDs, we amplified the coding sequences of HRJDs from
452 pUCIDT-HRJDs (Supplementary texts S1) by gene-specific primers with 3xFLAG tag at
453 5'-end of the forward primers, and the amplicons were then ligated into a pAc5-
454 STABLE2-neo (Addgene, 32426) [61] digested with EcoRI/XhoI by In-Fusion HD
455 Cloning Kit (Takara, 639649). Twenty-four hours after transfection, the cells were
456 washed with PBS and the medium was replaced with fresh Schneider's *Drosophila*
457 medium supplemented with 10% (v/v) heat-inactivated FBS, 100 U/mL penicillin, and
458 100 μg/mL streptomycin. Forty-eight hours after transfection, the cells were fixed with
459 4% paraformaldehyde (PFA) in PBS, washed with PBS containing 0.1% Triton X-100
460 (PBST), blocked in PBST with 5% normal donkey serum (PBSTn), and incubated with

461 primary antibodies in PBSTn overnight at 4 °C. The samples were then washed with
462 PBST, incubated for 1 h at room temperature with secondary antibodies and Hoechst
463 33342 suspended in PBSTn and washed again with PBST. Images were captured using
464 an LSM880 (Zeiss). The primary antibody used was a mouse anti-FLAG M2 monoclonal
465 antibody (1 : 2000, Sigma, F1804). The secondary antibodies used were Goat anti-Mouse
466 IgG2b Cross-Adsorbed Secondary Antibody, Alexa Fluor™ 555 (1:2000, Thermo Fisher
467 Scientific, A-21147). Hoechst 33342 (0.4 μM; Invitrogen, H3570) was used for nuclear
468 staining. Images were analyzed and edited using Fiji/ImageJ software (NIH).
469
470 **S2 cell western blotting**
471 To examine the expression of HRJDs, 2.5 × 10^5 cells were seeded in 24-well plates
472 containing Schneider's *Drosophila* medium supplemented with 10% (v/v) heat-
473 inactivated FBS, 100 U/mL penicillin, and 100 μg/mL streptomycin and were transfected
474 with 200 ng of pAc5-3xFLAG-HRJDs using Effectene Transfection Reagent (QIAGEN,
475 301427) following the manufacturer's protocol. Twenty-four hours after transfection, the
476 cells were washed with PBS and the medium was replaced with fresh Schneider's
477 *Drosophila* medium supplemented with 10% (v/v) heat-inactivated FBS, 100 U/mL
478 penicillin, and 100 μg/mL streptomycin. Forty-eight hours after transfection, the cells
479 were washed with PBS and lysed with 50 μL RIPA buffer supplemented with cOmplete
480 ULTRA EDTA-free protease inhibitor cocktail (Roche, 05892953001). The lysate was
481 sonicated and centrifuged at 20,000 g for 5 minutes. Protein concentration was
482 determined by BCA assay. The supernatant was mixed with SDS, boiled at 95 °C for 5
483 minutes, and subjected to western blotting.
484 Proteins were separated using SDS-PAGE and transferred onto Immobilon-P
485 PVDF membranes (Millipore, IPVH00010) for immunoblotting. Membranes were
486 blocked with 4% skimmed milk diluted in 1×Tris buffered saline containing 0.1% Tween-
487 20. Immunoblotting was performed using the below-mentioned antibodies, which were
488 diluted with 4% skim milk. The signals were visualized using Immobilon Western
489 Chemiluminescent HRP Substrate (Millipore, WBKLS0500) and FUSION SOLO. 7S.
490 EDGE (Vilber-Lourmat). Contrast and brightness adjustments were applied using the
491 Fiji/ImageJ software (NIH).
492 The primary antibody used was mouse anti-FLAG M2 monoclonal antibody
493 (1 : 5000, Sigma, F1804). Mouse anti-alpha tubulin (DM1A) monoclonal antibody

494 (1 : 5000, Sigma, T9026) was used as loading control. The secondary antibody used was
495 HRP-conjugated goat/rabbit/donkey anti-mouse IgG (1 : 10000, Promega, W402B).
496
497 **Drug treatment**
498 5 mM paraquat (Sigma, 856177) and 5% (w/v) DSS (MP Biomedicals, 160110) were
499 dissolved in 5% (w/v) sucrose solution. Filter paper (Whatman 3MM) was soaked with
500 400 µl of these reagents and placed into empty vials. For histological analyses, flies were
501 fed with the reagent solution for 1 day. For the survival assay, flies were transferred to
502 new vials and dead flies (determined by immobility and showing no response to tapping)
503 were counted every day. 5% sucrose was used for control feeding.
504
505 **Immunofluorescence**
506 Samples were dissected in 1×PBS and fixed in 4% PFA for 20 minutes (wing discs) and
507 30-45 minutes (adult midgut) at room temperature (RT), respectively. The following
508 primary antibodies were used with indicated dilution into 1×PBS containing 0.5% BSA
509 and 0.1% Triton X-100: rabbit anti-PH3 (Millipore 06-570, 1:1000), mouse anti-FLAG
510 (Sigma F1804, 1:1000), mouse anti-Dlg (DSHB 4F3, 1:100), rabbit anti-GFP (MBL 598,
511 1:500), rat anti-GFP (Nacalai tesque 04404-26, 1:400), rabbit anti-Tsp2A (Izumi et al.,
512 2016, 1:1000) [62], rabbit anti-Mesh (Izumi et al., 2012, 1:1000) [63], rabbit anti-Ssk
513 (Izumi et al., 2016, 1:1000) [62], chicken anti-β-galactosidase (Abcam ab9361, 1:500),
514 anti-cDcp1 (Cell Signaling Technology 9578, 1:200). After overnight incubation with
515 primary antibodies at 4°C, samples were incubated with fluorescent secondary antibodies
516 (Jackson ImmunoResearch and Invitrogen, 1:500) for 1 hour at RT. Hoechst 33342
517 (Invitrogen, final concentration: 10 µg/ml) was used to visualize DNA. Wing discs were
518 mounted as described previously [64, 65]. Samples were mounted in Slowfade Diamond
519 (ThermoFisher, S36963) and imaged with confocal microscopy Zeiss LSM880 or Zeiss
520 LSM980.
521
522 **Smurf assay**
523 We referred to Rera et al. (2012) for the Smurf assay conditions [35]. To prepare the
524 feeding medium, 100 µl of 50% (w/v) brilliant blue FCF (Wako, 027-12842, final 2.5%)
525 and 100 µl of 5% (w/v) sucrose were added to a vial containing 2 ml of cornmeal-agar
526 food. After mixing with a spatula, an Whatman 1 filter (1001-020) was put on the feeding

527 medium. Flies were fed with this medium at 25°C for one day, after which they were
528 transferred to a new vial containing cornmeal-agar food without blue dye to clean the
529 epidermis. Two hours after the transfer, Smurf phenotype was checked. We classified the
530 Smurf phenotype as blue dye leakage outside abdomen (thorax, head, legs).
531
532 **RT-qPCR**
533 Total RNA was purified from 10-15 midguts using the ReliaPrep RNA Tissue Miniprep
534 System (Promega). cDNA was made from 100 or 200 ng of RNA using PrimeScript RT
535 Reagent Kit (TaKaRa). Quantitative PCR was performed using TB Green Premix Ex
536 Taq II (TaKaRa) and the QuantStudio 6 Flex Real-Time PCR System (ThermoFisher).
537 RpL32 was used as an internal control. Primer sequences are listed in Table S2.
538
539 **Phylogenetic tree**
540 We created the phylogenetic tree of representative organisms using the NCBI taxonomy
541 browser (https://www.ncbi.nlm.nih.gov/Taxonomy/CommonTree/wwwcmt.cgi). The
542 species examined are *Amphimedon queenslandica* (Porifera), *Mnemiopsis leidyi*
543 (Ctenophora), *Trichoplax adhaerens* (Placozoa), *Hydra vulgaris* (Cnidaria), *Ptychodera*
544 *flava* (Hemichordata), *Acanthaster planci* (Echinodermata), *Branchiostoma floridae*
545 (Cephalochordata), *Ciona intestinalis* (Tunicata), *Danio rerio* (Teleostei), *Homo sapiens*,
546 *Mus musculus* (Mammalia), *Schmidtea mediterranea* (Platyhelminthes), *Caenorhabditis*
547 *elegans* (Nematoda), and *Drosophila melanogaster* (Arthropoda). These species, except
548 for *D. rerio, H. sapiens, M. musculus, C. elegans,* and *D. melanogaster,* are known to
549 have HRJDs and exhibit high regeneration ability [13]. The pictures were downloaded
550 from PhyloPic, and the color of some were changed from black to blue. Credits: Bennet
551 McComish (*B. floridae*), Malio Kodis (*M. leidyi*), and Markus A. Grohme (*S.*
552 *mediterranea*, https://www.phylopic.org/images/93f9611c-0cbd-4a14-92da-
553 004a4521e21f/schmidtea-mediterranea).
554
555 **Quantification of PH3 positive cells**
556 For wing discs, we counted PH3 positive cells in the pouch region, which develops into
557 the adult wing. After binarization, the number of PH3 positive cells was counted using
558 the Analyze Particles function in Fiji/ImageJ, and subsequently confirmed or corrected

559 by visual review of the images. For adult midguts, the number of PH3 positive cells in
560 the posterior midguts was manually counted.
561
562 **Quantification of junctional proteins**
563 To quantify junctional and cytoplasmic intensity, a line that was orthogonal to one side
564 of a cell was drawn, and then the plot profile was calculated for the line. We defined the
565 junctional intensity as the highest value in that prolife, and defined cytoplasmic intensity
566 as the value 20 pixels (~2.6 μm) away from the highest value. Three lines were drawn for
567 one cell and the average of the three was used to represent the junctional/cytoplasmic
568 ratio for the cell. Six polyploid cells were randomly selected from each image for
569 quantification.
570
571 **Quantification of reporter intensity**
572 The signal intensity of *puc-lacZ* and *10×STAT-GFP* reporters was quantified using
573 Fiji/ImageJ. The nuclei of large polyploid cells (for *puc-lacZ*) and Pros^{-} diploid cells (for
574 *10×STAT-GFP*) were selected as ROIs using the polygon selection tool. The reporter
575 intensity in each ROI was quantified using the Measure command.
576
577 **Quantification of nuclear size**
578 Nuclei of *esg-Gal4>UAS-GFP* positive cells were traced by the polygon selection tool
579 and added as ROI in Fiji/ImageJ. The size of each ROI was quantified using the Measure
580 command.
581
582 **Quantification of cell number**
583 Cell number was quantified using Fiji/ImageJ. To count the total cell number, Hoechst
584 signal was processed as following: (1) despeckle, (2) binarization, (3) fill hole, (4)
585 watershed, (5) analyze particle. The following cell number was manually counted using
586 the cell counter function: *esg>GFP*$^{+}$ cells, *Dl-lacZ*$^{+}$ cells, Pros^{+} cells, and cDcp1^{+} cells.
587
588 **Statistics**
589 Statistical analyses were performed using Excel and RStudio. Two tailed *t* tests were used
590 for comparisons between two groups. One-way ANOVAs with post hoc Tukey tests were
591 performed when comparing three or more groups. Log-rank tests were used for

comparison of survival curve. Significance is indicated in the Fig.s as follows: *P≤0.05, **P≤0.01, ***P≤0.001, Not Significant (N.S.): P>0.05. Bar graphs show mean ± standard error. Boxplots show median (thick line in the box), first and third quartiles (bottom and top of the box), minimum value (lower whisker), and maximum value (upper whisker). Dots in bar graphs and boxplots indicate individual values. Violin plots portray the distribution of individual values.

DECLARATIONS

Ethics approval and consent to participate

Not applicable.

Consent for publication

Not applicable.

Availability of data and materials

The datasets and *Drosophila* stocks used and/or analyzed during the current study are available from the corresponding author on reasonable request.

Competing interests

The authors declare that they have no competing interests.

Funding

This work was supported by JSPS/MEXT KAKENHI (grant numbers JP22J01430 to H.N., JP21H04774, JP23H04766, JP24H00567 to M.M., and JP17H06332, JP22H02762, JP23K18134, JP23H04696 to Y.N.), AMED-Aging (JP21gm5010001 to M.M.), AMED-PRIME (JP22gm6110025 to Y.N.), and Sadako O. Hirai Ban Award for Young Researchers (H.N.)

Author contributions

Conceptualization: H.N., Y.N.

Investigation: H.N., Y.A., T.N., E.T., J.U., Y.N.

Methodology: H.N., Y.N.

Validation: H.N., Y.A., T.N., E.T., J.U., T.M., M.M., Y.N.
Data curation: H.N., T.M., Y.N.
Writing – original draft: H.N., J.U., T.M., Y.N.
Writing – review & editing: H.N., Y.A., T.N., J.U., T.M., M.M., Y.N.
Supervision: M.M., Y.N.
Funding acquisition: H.N., T.M., M.M., Y.N.

Acknowledgements
We thank I. Miguel-Aliaga, N. Shinoda, M. Furuse, Y. Izumi, BDSC, Kyoto Stock Center, Transgenic RNAi Project (TRiP), and DSHB for fly stocks and reagents.

FIGURE LEGENDS

Figure 1. HRJD expression in whole body does not affect gross morphology.

(A) Phylogenetic tree of HRJD conservation. Green indicates species that possess HRJD gene(s) and gray indicates species that have lost HRJD gene(s). High regenerative ability indicates that the species can regenerate their whole body or anterior/posterior body parts, and low regenerative ability indicates that the species can only regenerate their appendage (limbs, tails, fins) or much smaller scale of tissues/organs. We referred to Cao et al., 2019 for the definition of regenerative ability [13].

(B) Protein sequence of HRJDs used in this study, which derived from *Dugesia japonica* (DjHRJDa/b, hereafter simply described as HRJDa/b). Conserved residues characteristic of the JmjC domain are shown.

(C) Schematics of genetic experiments for whole body induction of HRJDs. The Gal4-UAS system enables gene expression downstream of the UAS sequence, which is regulated by the transcription factor Gal4 [15]. In this case, the ubiquitously active *Act5C*

651 promoter is used for Gal4 expression.

652 (D) Representative images of mature adults for whole body expression of HRJDs.

653 (E) Whole body induction of HRJDs did not change body weight of mature adults.

654 (F) Representative images of adult wings.

655 (G) Whole body induction of HRJDs did not change wing size.

656 (H) Representative images for adult heads.

657 (I) Whole body induction of HRJDs did not change eye size of adult flies.

658 N.S., not significant: P>0.05. One-way ANOVAs with post hoc Tukey test. *n* indicates

659 the number of flies examined. See also Fig. S1.

660

661 **Figure 2. HRJD expression impedes tissue regeneration in the developing wind disc**

662 (A) Schematics of genetic ablation of the wing disc. TNF ligand *eiger* was overexpressed

663 in the wing pouch for 40 hrs during the larval stage.

664 (B) Wing regeneration was assessed in the adult stage by checking the size of wing (0%:

665 no wing, 100%: intact wing).

666 (C) Line graph for wing regeneration. Expression of HRJDa/b increased the rate of low

667 regeneration (0% and 25%) at the expense of the rate of full regeneration (100%).

668 (D-E) Representative images for PH3 staining of wing discs during regeneration at 48 hrs

669 after ablation (D). The number of PH3 positive cells is quantified in (E).

670 (F-G) Representative images for adult wings of *WP-QF>QUAS-HRJDa/b* flies under

671 homeostatic (non-regenerative) condition (F). The wing size is quantified in (G).

672 (H-I) Representative images for PH3 staining of wing discs (3rd instar larvae) during
673 normal development (H). The number of PH3 positive cells is quantified in (I).
674 N.S., not significant: P>0.05, ***P ≤0.001. Chi-square test (C) and one-way ANOVAs
675 with post hoc Tukey test (E, G, I). *n* indicates the number of wings (C, G) and wing discs
676 (E, I) examined. Scale bars: 20 μm.
677
678 **Figure 3. HRJDs expression compromises regeneration in the adult midgut**
679 (A) Schematics of the *Drosophila* adult midgut. The adult midgut is a pseudostratified
680 epithelium, in which intestinal stem cells (ISCs) generate both absorptive enterocytes
681 (ECs) and secretory enteroendocrine cells (EEs) through progenitor cell enteroblasts
682 (EBs) and EE progenitor cells (EEPs).
683 (B) Experimental scheme for ISC/EB specific induction of HRJDs under the *esg-Gal4*
684 driver in the adult stage. Adult flies were transferred to 29°C at Day 3 to induce HRJD
685 expression.
686 (C-E) Survival curve during paraquat (C), DSS (D), and sucrose (E) feeding.
687 (F) Representative images for PH3 staining upon paraquat feeding.
688 (G) Quantification of PH3 positive cells in posterior midguts.
689 N.S., not significant: P>0.05, *P<0.05, **P≤0.01. Log-rank test. *n* indicates the number
690 of flies (C-E) and midguts (G). Scale bars: 50 μm. See also Fig. S2.
691
692 **Figure 4. Post-developmental HRJD expression in ISC lineages extends organismal**
693 **lifespan**

694 (A-D) Survival curve for organismal lifespan by sex. HRJDs are induced by *esg*^{ts}-*Gal4*

695 (A and B) and *Act5C-Gal4* (C and D). For temporal regulation of HRJD induction using

696 *tub-Gal80*^{ts} (A and B), adult flies were transferred to 29°C at Day 3.

697 N.S., not significant: P>0.05, *P<0.05, **P≤0.01, ***P≤0.001, Log-rank tests. *n*

698 indicates the number of flies. See also Fig. S3.

699

700 **Figure 5. HRJD expression in adult ISCs/EBs suppress age-related gut barrier**

701 **dysfunction**

702 (A) *esg*^{ts}-mediated HRJD induction decreased Smurf(+) ratio at Day 30. The

703 representative images of the Smurf phenotype (leakage of blue dye throughout whole

704 body) is shown on the left.

705 (B-C) HRJD expression in adult ISCs/EBs maintained junctional localization of Dlg

706 protein in ECs, which is quantified in (C).

707 (D-I) HRJD expression in adult ISCs/EBs maintained junctional localization of Tsp2A

708 (D), Mesh (E), and Ssk (F) in ECs, which is quantified in (G-I).

709 (J) RT-qPCR of *puc* in the whole midgut. *esg*^{ts}-mediated induction of HRJDa significantly

710 repressed *puc*.

711 (K-L) *puc-lacZ* intensity in polyploid cells was decreased by HRJD expression (K), which

712 is quantified in (L).

713 *P<0.05, **P<0.01, ***P≤0.001, One-way ANOVAs with post hoc Tukey test. *n*

714 indicates the number of flies (A), cells (C, G, H, I, L), and biological replicates (J). Scale

715 bars: 50 μm.

716

717 **Figure 6. HRJD expression in adult ISCs/EBs improves stem cell functions in aged**

718 **midguts**

719 (A) Representative images for *esg-Gal4* positive cells in Day 30 midguts. HRJDs

720 suppressed mis-differentiation of esg^{+} cells (cellular enlargement with polyploid large

721 nuclei).

722 (B) Quantification of nuclear size of *esg-Gal4* positive cells.

723 (C-D) Representative images (C) and quantification (D) of PH3 positive cells in Day 30

724 posterior midguts.

725 (E) RT-qPCR of *Dl*, *nub*, and *pros* in Day 30 midguts. Expression levels were normalized

726 to those of GFP control.

727 (F-G) Cell type composition in aged midguts were assessed with esg^{ts}>*GFP* (ISC, EB,

728 and early EC), *Dl-lacZ* (ISC and EEP), and anti-Pros staining (EEP and EE). HRJD

729 expression in adult ISCs/EBs reduced the ratio of EB/early EC and increased the ratio of

730 EC (G).

731 (H-I) esg^{ts}-mediated HRJD induction enhanced STAT-GFP intensity in $Pros^{-}$ diploid cells

732 (ISCs/EBs), which is quantified in (I). Additionally, HRJDs suppressed STAT activation

733 in polyploid ECs (arrowheads).

734 N.S., not significant: P>0.05, *P≤0.05, **P≤0.01, ***P≤0.001, one-way ANOVAs with

735 post hoc Tukey test. *n* indicates the number of cells (B, I), guts (D, G), and biological

736 replicates (E). Scale bars: 50 μm.

737

738 **Figure 7. Graphical summary.**

739 Schematic model for the impact of HRJDs on intestinal homeostasis. In aged wildtype
740 midguts, ISCs over-proliferate, and their daughters fail to differentiate into mature ECs,
741 resulting in an accumulation of mis-differentiated cells (*esg*$^{+}$ large polyploid). HRJD
742 expression in adult ISCs/EBs further enhances ISC proliferation but suppresses mis-
743 differentiation likely through upregulation of JAK-STAT signaling, which results in
744 successful maintenance of the gut barrier and an extension of organismal lifespan.

745

746

747 ## Supplemental figure legends

748

749 **Figure S1. Expression and localization of HRJD proteins**

750 (A) Western blots of S2 cell samples upon transfection of 3×FLAG-HRJDa/b. Anti-FLAG
751 was used to detect 3×FLAG-HRJDa/b proteins and anti-tubulin was used as the loading
752 control. Expected molecular weight: 52.0 kDa for 3×FLAG-HRJDa, 52.9 kDa for
753 3×FLAG-HRJDb.

754 (B) Representative images of anti-FLAG staining using S2 cells transfected with
755 3×FLAG-HRJDa/b. Both HRJDa and HRJDb localized cytoplasm but not in nuclei. Scale
756 bar: 30 μm in wide-view images (left), 5 μm in magnified view images (yellow frames).

757 (C-D) Representative images of 3×FLAG-HRJDa/b localization in wing discs and adult
758 midguts. FLAG-tagged HRJDs were induced using *WP-Gal4* (C) or *esg-Gal4* (D). Scale
759 bars: 10 μm.

760

761 **Figure S2. Continuous expression of HRJDs throughout development hampers**

762 **intestinal regeneration**

763 (A-C) Organismal survival upon paraquat (A), DSS (B), and sucrose (C) feeding. Drug

764 feeding started at Day 7 after eclosion. HRJD induction using *esg-Gal4* throughout

765 development significantly decreased survival upon paraquat/DSS feeding.

766 (D) Expression of HRJDa using *esg-Gal4* decreased the number of PH3 positive cells in

767 the posterior midguts, while HRJDb did not significantly change PH3 positive cell

768 number.

769 N.S., not significant: P>0.05, **P≤0.01, ***P≤0.001, one-way ANOVAs with post hoc

770 Tukey test. *n* indicates the number of flies (A-C) and guts (D).

771

772 **Figure S3. Organismal lifespan of flies expressing HRJDs in ECs and ISC/EBs**

773 (A-F) Survival curve for organismal lifespan by sex. HRJDs are induced by *NP1-Gal4*

774 (A and B), *NP1^{ts}-Gal4* (C and D), and *esg-Gal4* (E and F).

775 N.S., not significant: P>0.05, ***P≤0.001, Log-rank tests. *n* indicates the number of flies.

776

777 **Figure S4. HRJD induction in adult ISCs/EBs promotes turnover of midgut**

778 **epithelial cells.**

779 (A) Representative images of esgFLPout aged midguts in which *esg*-lineage clones

780 express HRJDs together with GFP. Clones were induced 50 day after eclosion and traced

781 for 10 days (final 60-day old adults). Ssk was immunostained to compare the septate

782 junction of HRJD-expressing cells with that of wildtype cells, which is quantified in (B).

783 The magnified images of areas enclosed by squares are shown as images 1-5. Arrows

784 indicate GFP^+ polyploid adjacent cells in the control midgut.

785 (B) HRJD expression improved Ssk accumulation at septate junction not only in HRJD-

786 expressing cells (GFP^+/GFP^+), but also in wildtype cells (GFP^-/GFP^-).

787 (C) HRJD expression increased the ratio of GFP^+ cells and total cells, suggesting that old

788 ECs are more rapidly replaced by newly formed ECs.

789 (D) HRJD expression increased the ratio of GFP^+ polyploid cells and GFP^+ diploid cells,

790 suggesting that HRJDs increases the speed of differentiation to ECs.

791 (E) Quantification of PH3 positive cell number in Day 10 young posterior midguts. HRJD

792 induction with *esg-Gal4, tub-Gal80ts* driver did not change the quantity of mitotic cells.

793 (F-G) HRJD induction increased the ratio of $cDCP1^+$ cells in aged midguts (F), which is

794 quantified in (G).

795 (H) RT-qPCR of signaling ligands established as mitotic activators in the adult midgut.

796 N.S., not significant: $P>0.05$, $*P\leq0.05$, $**P\leq0.01$, $***P\leq0.001$, one-way ANOVAs with

797 post hoc Tukey test. *n* indicates the number of cells (B), midguts (C, D, E and G), and

798 biological replicates (H). Scale bar: 50 µm or 25 µm (magnified images 1-5).

799

800

801 **Table S1. Detailed genotypes in each experiment**

Fig.	Panel	Genotype
Fig. 1	**D-I**	*w;; Act5C-Gal4 / +*
		w; UAS-GFP / +; Act5C-Gal4 / UAS-HRJDb

		w;; Act5C-Gal4 / UAS-HRJDa
		w;; Act5C-Gal4 / UAS-HRJDb
Fig. 2	**A-E**	*w; rn-Gal4, tub-Gal80ts, UAS-egr / +; WP-QF2 / +*
		w; rn-Gal4, tub-Gal80ts, UAS-egr / +; WP-QF2 / QUAS-HRJDa
		w; rn-Gal4, tub-Gal80ts, UAS-egr / +; WP-QF2 / QUAS-HRJDb
	F-I	*w;; WP-QF2 / +*
		w;; WP-QF2 / QUAS-HRJDa
		w;; WP-QF2 / QUAS-HRJDb
Fig. 3	**C-G**	*w; esg-Gal4, tub-Gal80ts / UAS-GFP*
		w; esg-Gal4, tub-Gal80ts / +; UAS-HRJDa / +
		w; esg-Gal4, tub-Gal80ts / +; UAS-HRJDb / +
Fig. 4	**A-B**	*w; esg-Gal4, tub-Gal80ts / UAS-GFP*
		w; esg-Gal4, tub-Gal80ts / +; UAS-HRJDa / +
		w; esg-Gal4, tub-Gal80ts / +; UAS-HRJDb / +
	C-D	*w; UAS-GFP / +; Act5C-Gal4 / +*
		w;; Act5C-Gal4 / UAS-HRJDa
		w;; Act5C-Gal4 / UAS-HRJDb
Fig. 5	**A-I**	*w; esg-Gal4, tub-Gal80ts / UAS-GFP*
		w; esg-Gal4, tub-Gal80ts / +; UAS-HRJDa / +
		w; esg-Gal4, tub-Gal80ts / +; UAS-HRJDb / +
	J	*w, Su(H)GBE-lacZ / w; esg-Gal4, tub-Gal80ts / UAS-GFP*
		w, Su(H)GBE-lacZ / w; esg-Gal4, tub-Gal80ts / +; UAS-HRJDa / +
		w, Su(H)GBE-lacZ / w; esg-Gal4, tub-Gal80ts / +; UAS-HRJDb / +
	K-L	*w; esg-Gal4, tub-Gal80ts, UAS-GFP / +; puc-lacZ / +*
		w; esg-Gal4, tub-Gal80ts, UAS-GFP / +; puc-lacZ / UAS-HRJDa
		w; esg-Gal4, tub-Gal80ts, UAS-GFP / +; puc-lacZ / UAS-HRJDb
Fig. 6	**A-E**	*w; esg-Gal4, tub-Gal80ts, UAS-GFP / +*
		w; esg-Gal4, tub-Gal80ts, UAS-GFP / +; UAS-HRJDa / +
		w; esg-Gal4, tub-Gal80ts, UAS-GFP / +; UAS-HRJDb / +
	F-G	*w; esg-Gal4, tub-Gal80ts, UAS-GFP / +; Dl-lacZ / +*
		w; esg-Gal4, tub-Gal80ts, UAS-GFP / +; Dl-lacZ / UAS-HRJDa
		w; esg-Gal4, tub-Gal80ts, UAS-GFP / +; Dl-lacZ / UAS-HRJDb

	H-I	*w; esg-Gal4, tub-Gal80ts, UAS-GFP / +; 10×STAT-GFP / +*
		w; esg-Gal4, tub-Gal80ts, UAS-GFP / +; 10×STAT-GFP / UAS-HRJDa
		w; esg-Gal4, tub-Gal80ts, UAS-GFP / +; 10×STAT-GFP / UAS-HRJDb
Fig. S1	**C**	*w;; WP-Gal4 / +*
		w;; WP-Gal4 / UAS-FLAG-HRJDa
		w;; WP-Gal4 / UAS-FLAG-HRJDb
	D	*w; esg-Gal4, tub-Gal80ts, UAS-GFP / +*
		w; esg-Gal4, tub-Gal80ts, UAS-GFP / +; UAS-FLAG-HRJDa / +
		w; esg-Gal4, tub-Gal80ts, UAS-GFP / +; UAS-FLAG-HRJDb / +
Fig. S2	**All**	*w; esg-Gal4 / UAS-GFP*
		w; esg-Gal4 / +; UAS-HRJDa / +
		w; esg-Gal4 / +; UAS-HRJDb / +
Fig. S3	**A-B**	*w; NP1-Gal4 / UAS-GFP*
		w; NP1-Gal4 / +; UAS-HRJDa / +
		w; NP1-Gal4 / +; UAS-HRJDb / +
	C-D	*w; NP1-Gal4, tub-Gal80ts / UAS-GFP*
		w; NP1-Gal4, tub-Gal80ts / +; UAS-HRJDa / +
		w; NP1-Gal4, tub-Gal80ts / +; UAS-HRJDb / +
	E-F	*w; esg-Gal4 / UAS-GFP*
		w; esg-Gal4 / +; UAS-HRJDa / +
		w; esg-Gal4 / +; UAS-HRJDb / +
Fig. S4	**A-D**	*w; esg-Gal4, UAS-GFP, tub-Gal80ts / +; UAS-FLP, Act5C-FRT-CD2-FRT-Gal4 / +*
		w; esg-Gal4, UAS-GFP, tub-Gal80ts / +; UAS-FLP, Act5C-FRT-CD2-FRT-Gal4 / UAS-HRJDa
		w; esg-Gal4, UAS-GFP, tub-Gal80ts / +; UAS-FLP, Act5C-FRT-CD2-FRT-Gal4 / UAS-HRJDb
	E-G	*w; esg-Gal4, tub-Gal80ts, UAS-GFP / +*
		w; esg-Gal4, tub-Gal80ts, UAS-GFP / +; UAS-HRJDa / +
		w; esg-Gal4, tub-Gal80ts, UAS-GFP / +; UAS-HRJDb / +
	H	*w, Su(H)GBE-lacZ / w; esg-Gal4, tub-Gal80ts / UAS-GFP*
		w, Su(H)GBE-lacZ / w; esg-Gal4, tub-Gal80ts / +; UAS-HRJDa / +

		w, Su(H)GBE-lacZ / w; esg-Gal4, tub-Gal80ts / +; UAS-HRJDb / +

Table S2. Primer sequences

Supplementary texts S1. Sequences for pUCIDT-HRJDa and pUCIDT-HRJDb

Abbreviations

i-cell: interstitial cell
HRJD: highly regenerative species-specific JmjC domain-encoding gene
PH3: phospho-histone H3
ISC: intestinal stem cell
EB: enteroblast
EEP: enteroendocrine progenitor
EC: enterocyte
EE: enteroendocrine cell
DSS: dextran sulfate sodium
puc: puckered
Dl: Delta
Jarid2: Jumonji, AT rich interactive domain 2

References

1. Bely AE, Nyberg KG. Evolution of animal regeneration: re-emergence of a field. Trends Ecol Evol. 2010;25:161–70.
2. Poss KD. Advances in understanding tissue regenerative capacity and mechanisms in animals. Nat Rev Genet. 2010;11:710–22.
3. Tiozzo S, Copley RR. Reconsidering regeneration in metazoans: an evo-devo approach. Front Ecol Evol. 2015;3.
4. Bideau L, Kerner P, Hui J, Vervoort M, Gazave E. Animal regeneration in the era of transcriptomics. Cell Mol Life Sci. 2021;78:3941–56.
5. Fujita S, Kuranaga E, Nakajima Y. Regeneration Potential of Jellyfish: Cellular Mechanisms and Molecular Insights. Genes. 2021;12:758.
6. Piraino S, Boero F, Aeschbach B, Schmid V. Reversing the Life Cycle: Medusae

832 Transforming into Polyps and Cell Transdifferentiation in *Turritopsis nutricula* (Cnidaria,
833 Hydrozoa). Biol Bull. 1996;190:302–12.
834 7. Varley Á, Horkan HR, McMahon ET, Krasovec G, Frank U. Pluripotent, germ cell
835 competent adult stem cells underlie cnidarian regenerative ability and clonal growth. Curr
836 Biol. 2023;33:1883-1892.e3.
837 8. Gazave E, Röttinger E. 7th Euro Evo Devo meeting: Report on the "Evolution of
838 regeneration in Metazoa" symposium. J Exp Zoolog B Mol Dev Evol. 2021;336:89–93.
839 9. Kumar A, Godwin JW, Gates PB, Garza-Garcia AA, Brockes JP. Molecular Basis for
840 the Nerve Dependence of Limb Regeneration in an Adult Vertebrate. Science.
841 2007;318:772–7.
842 10. Da Silva SM, Gates PB, Brockes JP. The Newt Ortholog of CD59 Is Implicated in
843 Proximodistal Identity during Amphibian Limb Regeneration. Dev Cell. 2002;3:547–55.
844 11. Looso M, Preussner J, Sousounis K, Bruckskotten M, Michel CS, Lignelli E, et al. A
845 de novo assembly of the newt transcriptome combined with proteomic validation
846 identifies new protein families expressed during tissue regeneration. Genome Biol.
847 2013;14:R16.
848 12. Mehta AS, Deshpande P, Chimata AV, Tsonis PA, Singh A. Newt regeneration genes
849 regulate Wingless signaling to restore patterning in Drosophila eye. iScience.
850 2021;24:103166.
851 13. Cao P-L, Kumagai N, Inoue T, Agata K, Makino T. JmjC Domain-Encoding Genes
852 Are Conserved in Highly Regenerative Metazoans and Are Associated with Planarian
853 Whole-Body Regeneration. Genome Biol Evol. 2019;11:552–64.
854 14. Umesono Y, Tasaki J, Nishimura Y, Hrouda M, Kawaguchi E, Yazawa S, et al. The
855 molecular logic for planarian regeneration along the anterior–posterior axis. Nature.
856 2013;500:73–6.
857 15. Brand AH, Perrimon N. Targeted gene expression as a means of altering cell fates
858 and generating dominant phenotypes. Development. 1993;118:401–15.
859 16. Hariharan IK, Serras F. Imaginal disc regeneration takes flight. Curr Opin Cell Biol.
860 2017;48:10–6.
861 17. Smith-Bolton RK, Worley MI, Kanda H, Hariharan IK. Regenerative Growth in
862 Drosophila Imaginal Discs Is Regulated by Wingless and Myc. Dev Cell. 2009;16:797–
863 809.
864 18. Worley MI, Alexander LA, Hariharan IK. CtBP impedes JNK- and Upd/STAT-driven

865 cell fate misspecifications in regenerating Drosophila imaginal discs. eLife.
866 2018;7:e30391.
867 19. Potter CJ, Tasic B, Russler EV, Liang L, Luo L. The Q System: A Repressible Binary
868 System for Transgene Expression, Lineage Tracing, and Mosaic Analysis. Cell.
869 2010;141:536–48.
870 20. Riabinina O, Luginbuhl D, Marr E, Liu S, Wu MN, Luo L, et al. Improved and
871 expanded Q-system reagents for genetic manipulations. Nat Methods. 2015;12:219–22.
872 21. Nagai H, Miura M, Nakajima Y. Cellular mechanisms underlying adult tissue
873 plasticity in Drosophila. Fly (Austin). 2022;16:190–206.
874 22. Miguel-Aliaga I, Jasper H, Lemaitre B. Anatomy and Physiology of the Digestive
875 Tract of *Drosophila melanogaster*. Genetics. 2018;210:357–96.
876 23. Zhang P, Edgar BA. Insect Gut Regeneration. Cold Spring Harb Perspect Biol.
877 2021;:a040915.
878 24. Jasper H. Intestinal Stem Cell Aging: Origins and Interventions. Annu Rev Physiol.
879 2020;82:203–26.
880 25. Buchon N, Broderick NA, Chakrabarti S, Lemaitre B. Invasive and indigenous
881 microbiota impact intestinal stem cell activity through multiple pathways in *Drosophila*.
882 Genes Dev. 2009;23:2333–44.
883 26. Jiang H, Patel PH, Kohlmaier A, Grenley MO, McEwen DG, Edgar BA.
884 Cytokine/Jak/Stat Signaling Mediates Regeneration and Homeostasis in the Drosophila
885 Midgut. Cell. 2009;137:1343–55.
886 27. Biteau B, Hochmuth CE, Jasper H. JNK Activity in Somatic Stem Cells Causes Loss
887 of Tissue Homeostasis in the Aging Drosophila Gut. Cell Stem Cell. 2008;3:442–55.
888 28. Amcheslavsky A, Jiang J, Ip YT. Tissue Damage-Induced Intestinal Stem Cell
889 Division in Drosophila. Cell Stem Cell. 2009;4:49–61.
890 29. Jiang H, Edgar BA. EGFR signaling regulates the proliferation of *Drosophila* adult
891 midgut progenitors. Development. 2009;136:483–93.
892 30. Houtz P, Bonfini A, Bing X, Buchon N. Recruitment of Adult Precursor Cells
893 Underlies Limited Repair of the Infected Larval Midgut in Drosophila. Cell Host Microbe.
894 2019;26:412-425.e5.
895 31. Rera M, Bahadorani S, Cho J, Koehler CL, Ulgherait M, Hur JH, et al. Modulation of
896 Longevity and Tissue Homeostasis by the Drosophila PGC-1 Homolog. Cell Metab.
897 2011;14:623–34.

898 32. Thevaranjan N, Puchta A, Schulz C, Naidoo A, Szamosi JC, Verschoor CP, et al.
899 Age-Associated Microbial Dysbiosis Promotes Intestinal Permeability, Systemic
900 Inflammation, and Macrophage Dysfunction. Cell Host Microbe. 2017;21:455-466.e4.
901 33. Nagai H, Tatara H, Tanaka-Furuhashi K, Kurata S, Yano T. Homeostatic Regulation
902 of ROS-Triggered Hippo-Yki Pathway via Autophagic Clearance of Ref(2)P/p62 in the
903 Drosophila Intestine. Dev Cell. 2021;56:81-94.e10.
904 34. Egge N, Arneaud SLB, Wales P, Mihelakis M, McClendon J, Fonseca RS, et al. Age-
905 Onset Phosphorylation of a Minor Actin Variant Promotes Intestinal Barrier Dysfunction.
906 Dev Cell. 2019;51:587-601.e7.
907 35. Rera M, Clark RI, Walker DW. Intestinal barrier dysfunction links metabolic and
908 inflammatory markers of aging to death in Drosophila. Proc Natl Acad Sci.
909 2012;109:21528–33.
910 36. Resnik-Docampo M, Koehler CL, Clark RI, Schinaman JM, Sauer V, Wong DM, et
911 al. Tricellular junctions regulate intestinal stem cell behaviour to maintain homeostasis.
912 Nat Cell Biol. 2017;19:52–9.
913 37. Salazar AM, Resnik-Docampo M, Ulgherait M, Clark RI, Shirasu-Hiza M, Jones DL,
914 et al. Intestinal Snakeskin Limits Microbial Dysbiosis during Aging and Promotes
915 Longevity. iScience. 2018;9:229–43.
916 38. Izumi Y, Furuse K, Furuse M. Septate junctions regulate gut homeostasis through
917 regulation of stem cell proliferation and enterocyte behavior in *Drosophila*. J Cell Sci.
918 2019;:jcs.232108.
919 39. Chen H, Zheng X, Zheng Y. Age-Associated Loss of Lamin-B Leads to Systemic
920 Inflammation and Gut Hyperplasia. Cell. 2014;159:829–43.
921 40. Korzelius J, Naumann SK, Loza-Coll MA, Chan JS, Dutta D, Oberheim J, et al.
922 *Escargot* maintains stemness and suppresses differentiation in *Drosophila* intestinal stem
923 cells. EMBO J. 2014;33:2967–82.
924 41. Li Y, Pang Z, Huang H, Wang C, Cai T, Xi R. Transcription Factor Antagonism
925 Controls Enteroendocrine Cell Specification from Intestinal Stem Cells. Sci Rep.
926 2017;7:988.
927 42. Zhou F, Rasmussen A, Lee S, Agaisse H. The UPD3 cytokine couples environmental
928 challenge and intestinal stem cell division through modulation of JAK/STAT signaling
929 in the stem cell microenvironment. Dev Biol. 2013;373:383–93.
930 43. Zhai Z, Boquete J-P, Lemaitre B. A genetic framework controlling the differentiation

931 of intestinal stem cells during regeneration in Drosophila. PLOS Genet.
932 2017;13:e1006854.
933 44. Hudry B, De Goeij E, Mineo A, Gaspar P, Hadjieconomou D, Studd C, et al. Sex
934 Differences in Intestinal Carbohydrate Metabolism Promote Food Intake and Sperm
935 Maturation. Cell. 2019;178:901-918.e16.
936 45. Liang J, Balachandra S, Ngo S, O'Brien LE. Feedback regulation of steady-state
937 epithelial turnover and organ size. Nature. 2017;548:588–91.
938 46. Antonello ZA, Reiff T, Ballesta-Illan E, Dominguez M. Robust intestinal homeostasis
939 relies on cellular plasticity in enteroblasts mediated by miR-8–Escargot switch. EMBO J.
940 2015;34:2025–41.
941 47. Clark RI, Salazar A, Yamada R, Fitz-Gibbon S, Morselli M, Alcaraz J, et al. Distinct
942 Shifts in Microbiota Composition during Drosophila Aging Impair Intestinal Function
943 and Drive Mortality. Cell Rep. 2015;12:1656–67.
944 48. Wang L, Ryoo HD, Qi Y, Jasper H. PERK Limits Drosophila Lifespan by Promoting
945 Intestinal Stem Cell Proliferation in Response to ER Stress. PLOS Genet.
946 2015;11:e1005220.
947 49. Hu X, Li J, Fu M, Zhao X, Wang W. The JAK/STAT signaling pathway: from bench
948 to clinic. Signal Transduct Target Ther. 2021;6:402.
949 50. Markolovic S, Leissing TM, Chowdhury R, Wilkins SE, Lu X, Schofield CJ.
950 Structure–function relationships of human JmjC oxygenases—demethylases versus
951 hydroxylases. Curr Opin Struct Biol. 2016;41:62–72.
952 51. Suong DNA, Shimaji K, Pyo J-H, Park J-S, Yoshida H, Yoo M-A, et al.
953 Overexpression of dJmj differentially affects intestinal stem cells and differentiated
954 enterocytes. Cell Signal. 2018;42:194–210.
955 52. Hsia DA, Tepper CG, Pochampalli MR, Hsia EYC, Izumiya C, Huerta SB, et al.
956 KDM8, a H3K36me2 histone demethylase that acts in the cyclin A1 coding region to
957 regulate cancer cell proliferation. Proc Natl Acad Sci. 2010;107:9671–6.
958 53. Shalaby NA, Sayed R, Zhang Q, Scoggin S, Eliazer S, Rothenfluh A, et al. Systematic
959 discovery of genetic modulation by Jumonji histone demethylases in Drosophila. Sci Rep.
960 2017;7:5240.
961 54. Klose RJ, Kallin EM, Zhang Y. JmjC-domain-containing proteins and histone
962 demethylation. Nat Rev Genet. 2006;7:715–27.
963 55. Nakajima Y. Mitotic spindle orientation in epithelial homeostasis and plasticity. J

964 Biochem (Tokyo). 2018;164:277–84.
965 56. Goulas S, Conder R, Knoblich JA. The Par Complex and Integrins Direct Asymmetric
966 Cell Division in Adult Intestinal Stem Cells. Cell Stem Cell. 2012;11:529–40.
967 57. Hu DJ-K, Jasper H. Control of Intestinal Cell Fate by Dynamic Mitotic Spindle
968 Repositioning Influences Epithelial Homeostasis and Longevity. Cell Rep.
969 2019;28:2807-2823.e5.
970 58. Brunet A, Goodell MA, Rando TA. Ageing and rejuvenation of tissue stem cells and
971 their niches. Nat Rev Mol Cell Biol. 2023;24:45–62.
972 59. Campisi J, Kapahi P, Lithgow GJ, Melov S, Newman JC, Verdin E. From discoveries
973 in ageing research to therapeutics for healthy ageing. Nature. 2019;571:183–92.
974 60. Kashio S, Obata F, Zhang L, Katsuyama T, Chihara T, Miura M. Tissue
975 nonautonomous effects of fat body methionine metabolism on imaginal disc repair in
976 *Drosophila*. Proc Natl Acad Sci. 2016;113:1835–40.
977 61. González M, Martín-Ruíz I, Jiménez S, Pirone L, Barrio R, Sutherland JD. Generation
978 of stable Drosophila cell lines using multicistronic vectors. Sci Rep. 2011;1:75.
979 62. Izumi Y, Motoishi M, Furuse K, Furuse M. A tetraspanin regulates septate junction
980 formation in *Drosophila* midgut. J Cell Sci. 2016;:jcs.180448.
981 63. Izumi Y, Yanagihashi Y, Furuse M. A novel protein complex, mesh-ssk, is required
982 for septate junction formation in *drosophila* midgut. J Cell Sci. 2012;:jcs.112243.
983 64. Nakajima Y. Analysis of Epithelial Architecture and Planar Spindle Orientation in
984 the Drosophila Wing Disc. In: Turksen K, editor. Stem Cell Renewal and Cell-Cell
985 Communication. Methods Mol Biol. 2021;2346:51–62.
986 65. Nakajima Y, Lee ZT, McKinney SA, Swanson SK, Florens L, Gibson MC. Junctional
987 tumor suppressors interact with 14-3-3 proteins to control planar spindle alignment. J Cell
988 Biol. 2019;218:1824–38.
989

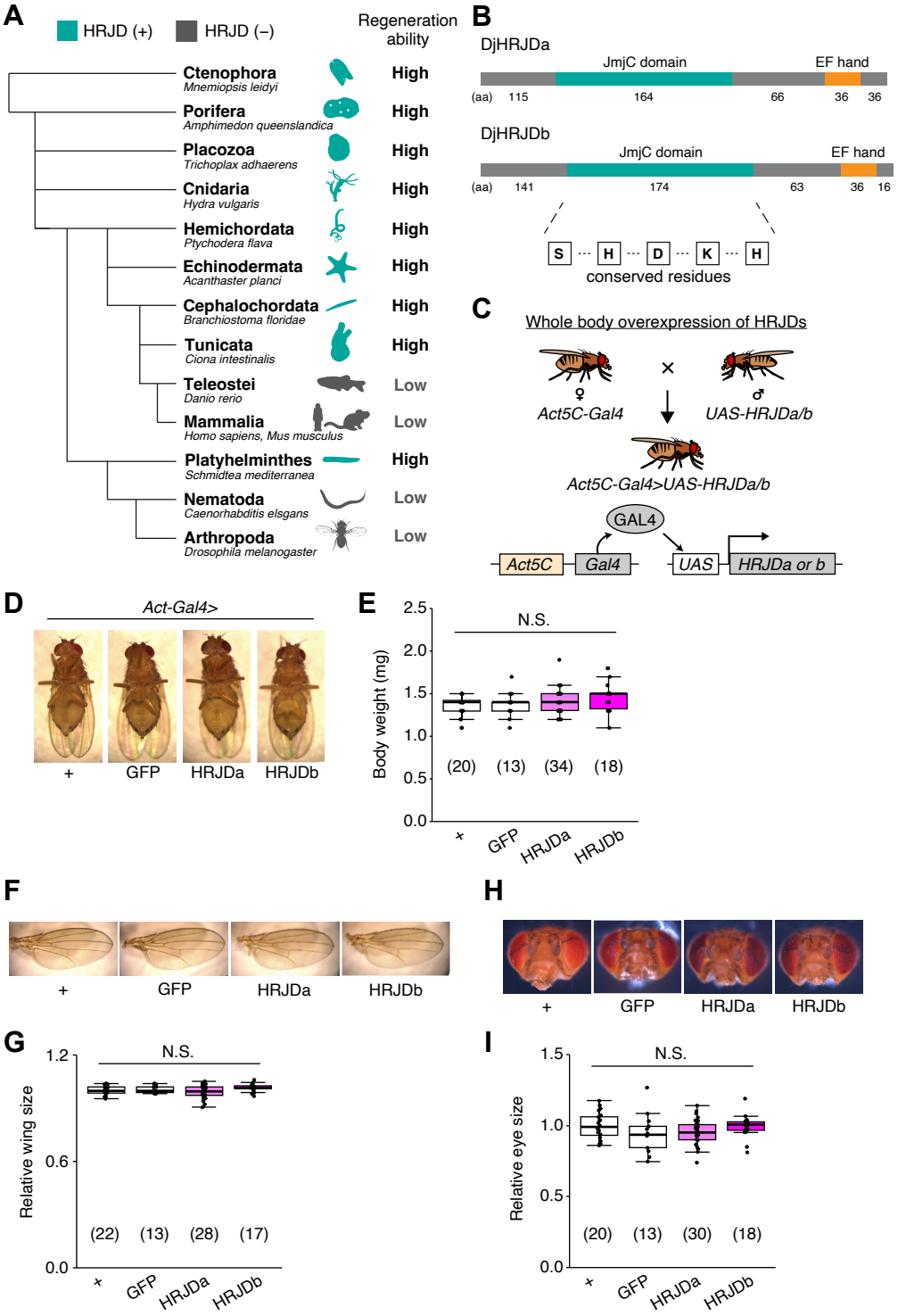
A
HRJD (+)
HRJD (–)
Regeneration ability
Ctenophora
Mnemiopsis leidyi
High
Porifera
Amphimedon queenslandica
High
Placozoa
Trichoplax adhaerens
High
Cnidaria
Hydra vulgaris
High
Hemichordata
Ptychodera flava
High
Echinodermata
Acanthaster planci
High
Cephalochordata
Branchiostoma floridae
High
Tunicata
Ciona intestinalis
High
Teleostei
Danio rerio
Low
Mammalia
Homo sapiens, Mus musculus
Low
Platyhelminthes
Schmidtea mediterranea
High
Nematoda
Caenorhabditis elsgans
Low
Arthropoda
Drosophila melanogaster
Low
B
DjHRJDa
JmjC domain
EF hand
(aa) 115 164 66 36 36
DjHRJDb
JmjC domain
EF hand
(aa) 141 174 63 36 16
S H D K H
conserved residues
C
Whole body overexpression of HRJDs
Act5C-Gal4
UAS-HRJDa/b
Act5C-Gal4>UAS-HRJDa/b
GAL4
Act5C
Gal4
UAS
HRJDa or b
D
Act-Gal4>
+
GFP
HRJDa
HRJDb
E
N.S.
Body weight (mg)
2.5
2.0
1.5
1.0
0.5
0.0
(20) (13) (34) (18)
+
GFP
HRJDa
HRJDb
F
+
GFP
HRJDa
HRJDb
H
+
GFP
HRJDa
HRJDb
G
N.S.
Relative wing size
1.2
0.6
0.0
(22) (13) (28) (17)
+
GFP
HRJDa
HRJDb
I
N.S.
Relative eye size
1.5
1.0
0.5
0.0
(20) (13) (30) (18)
+
GFP
HRJDa
HRJDb

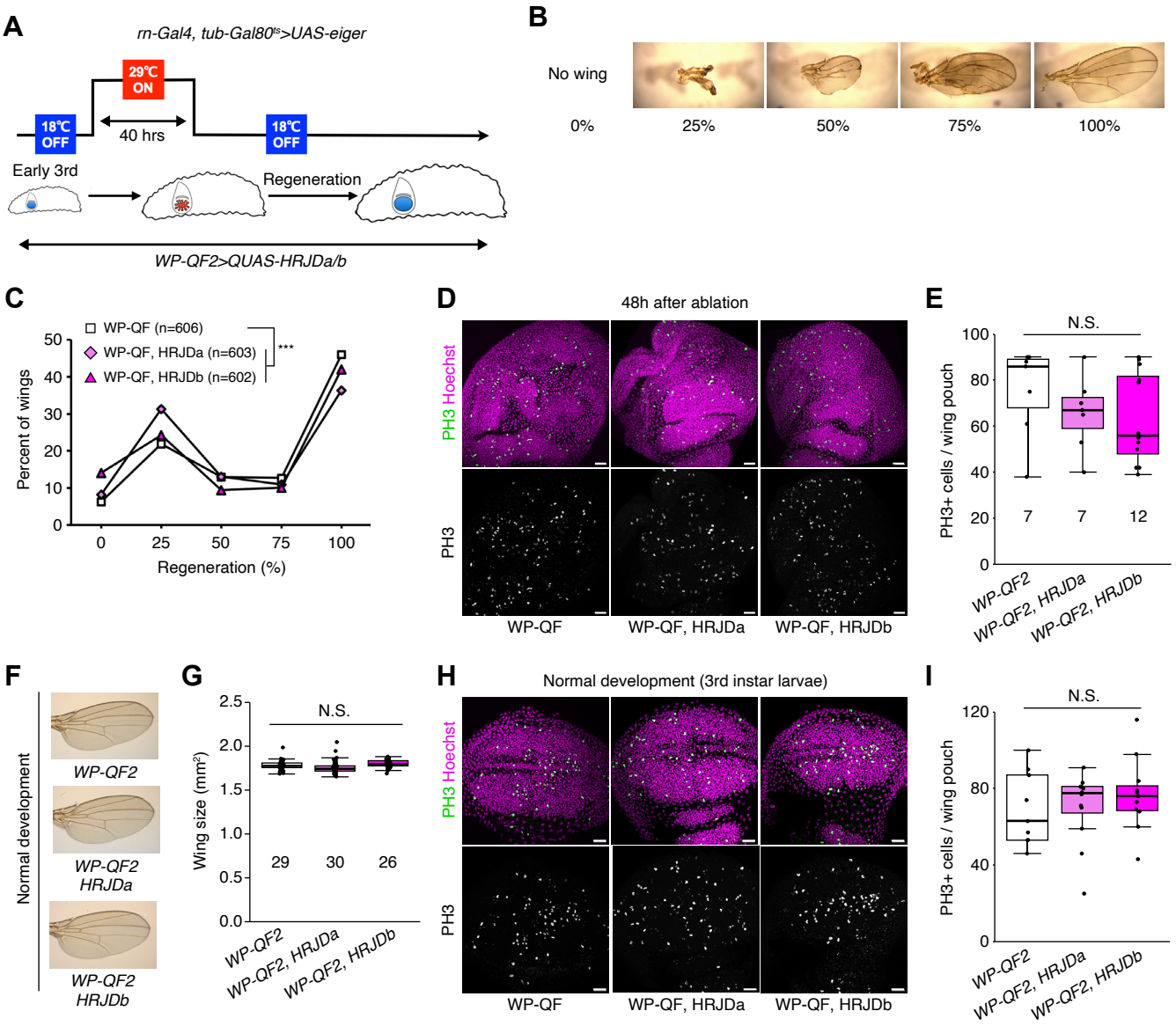
A
rn-Gal4, tub-Gal80ts>UAS-eiger
29℃ ON
18℃ OFF
40 hrs
18℃ OFF
Early 3rd
Regeneration
WP-QF2>QUAS-HRJDa/b
B
No wing
0%
25%
50%
75%
100%
C
WP-QF (n=606)
WP-QF, HRJDa (n=603)
WP-QF, HRJDb (n=602)
***
Percent of wings
Regeneration (%)
D
48h after ablation
PH3 Hoechst
PH3
WP-QF
WP-QF, HRJDa
WP-QF, HRJDb
E
N.S.
PH3+ cells / wing pouch
7
7
12
WP-QF2
WP-QF2, HRJDa
WP-QF2, HRJDb
F
Normal development
WP-QF2
WP-QF2 HRJDa
WP-QF2 HRJDb
G
N.S.
Wing size (mm2)
29
30
26
WP-QF2
WP-QF2, HRJDa
WP-QF2, HRJDb
H
Normal development (3rd instar larvae)
PH3 Hoechst
PH3
WP-QF
WP-QF, HRJDa
WP-QF, HRJDb
I
N.S.
PH3+ cells / wing pouch
WP-QF2
WP-QF2, HRJDa
WP-QF2, HRJDb

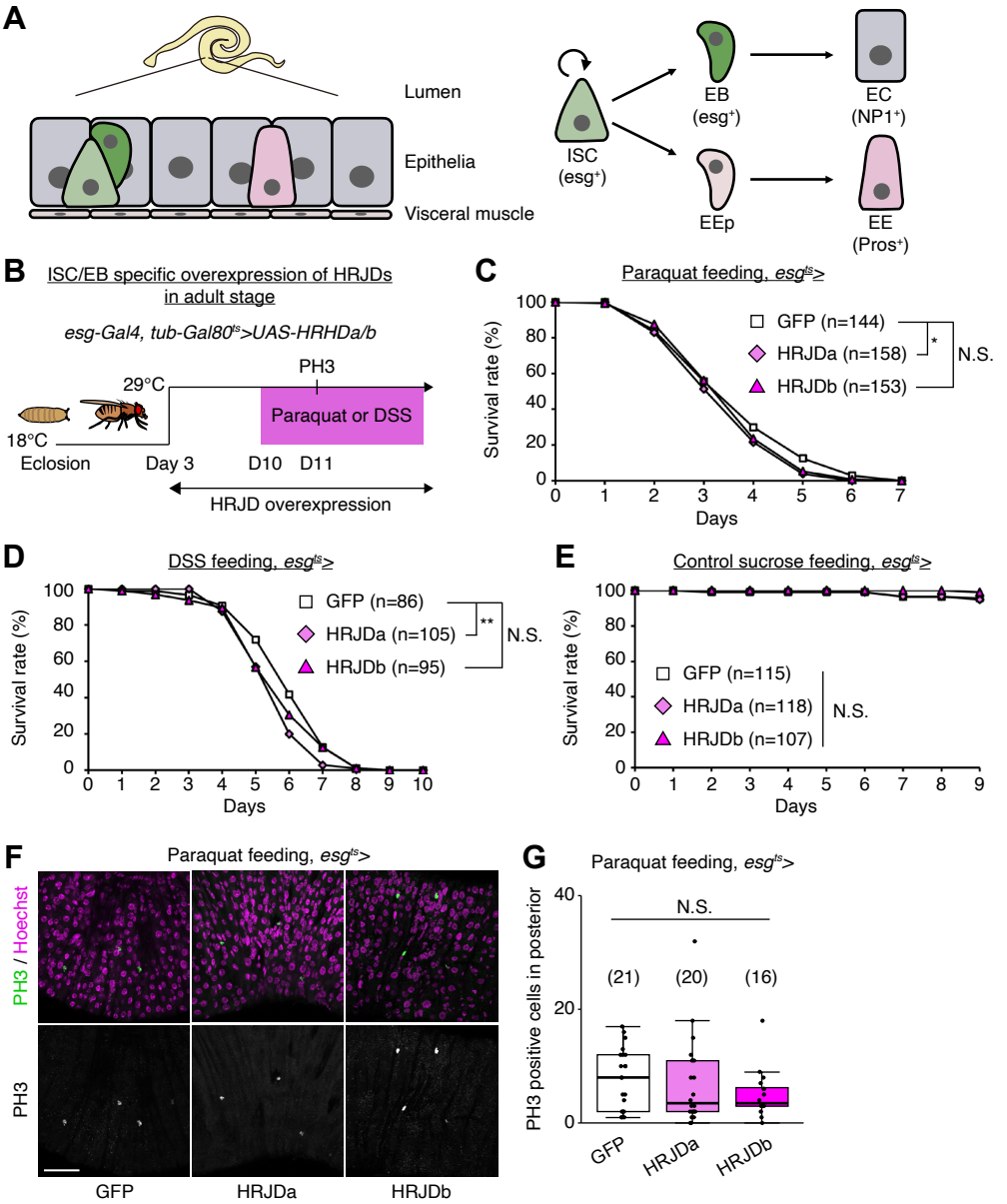
A
Lumen
Epithelia
Visceral muscle
ISC
(esg+)
EB
(esg+)
EC
(NP1+)
EEp
EE
(Pros+)
B
ISC/EB specific overexpression of HRJDs in adult stage
esg-Gal4, tub-Gal80ts>UAS-HRHDa/b
29°C
18°C
Eclosion
Day 3
PH3
Paraquat or DSS
D10
D11
HRJD overexpression
C
Paraquat feeding, esgts>
Survival rate (%)
Days
GFP (n=144)
HRJDa (n=158)
HRJDb (n=153)
*
N.S.
D
DSS feeding, esgts>
GFP (n=86)
HRJDa (n=105)
HRJDb (n=95)
**
N.S.
E
Control sucrose feeding, esgts>
GFP (n=115)
HRJDa (n=118)
HRJDb (n=107)
N.S.
F
Paraquat feeding, esgts>
PH3 / Hoechst
PH3
GFP
HRJDa
HRJDb
G
Paraquat feeding, esgts>
PH3 positive cells in posterior
N.S.
(21)
(20)
(16)
GFP
HRJDa
HRJDb

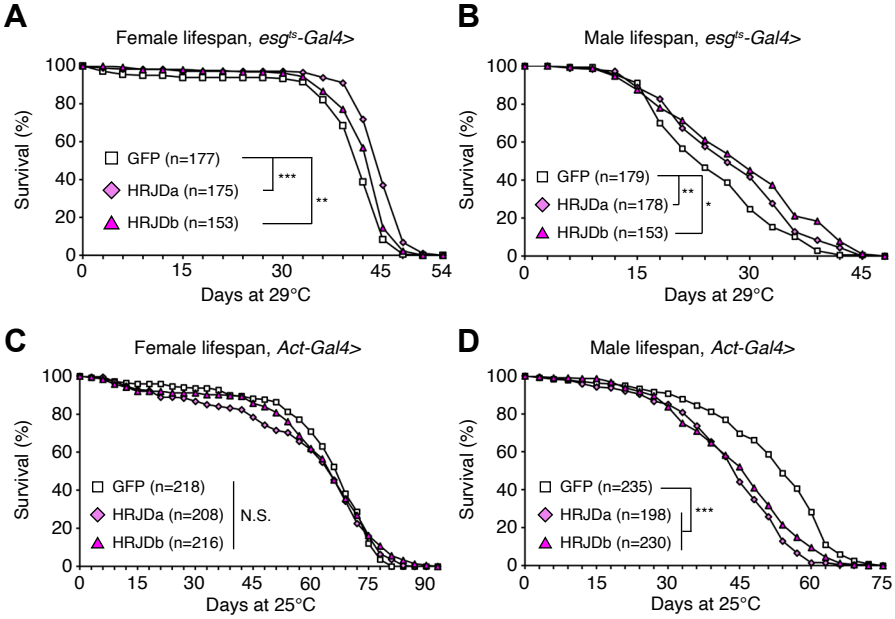
A
Female lifespan, esg^ts-Gal4>
Survival (%)
Days at 29°C
GFP (n=177)
HRJDa (n=175)
HRJDb (n=153)
***
**
B
Male lifespan, esg^ts-Gal4>
Survival (%)
Days at 29°C
GFP (n=179)
HRJDa (n=178)
HRJDb (n=153)
**
*
C
Female lifespan, Act-Gal4>
Survival (%)
Days at 25°C
GFP (n=218)
HRJDa (n=208)
HRJDb (n=216)
N.S.
D
Male lifespan, Act-Gal4>
Survival (%)
Days at 25°C
GFP (n=235)
HRJDa (n=198)
HRJDb (n=230)
***

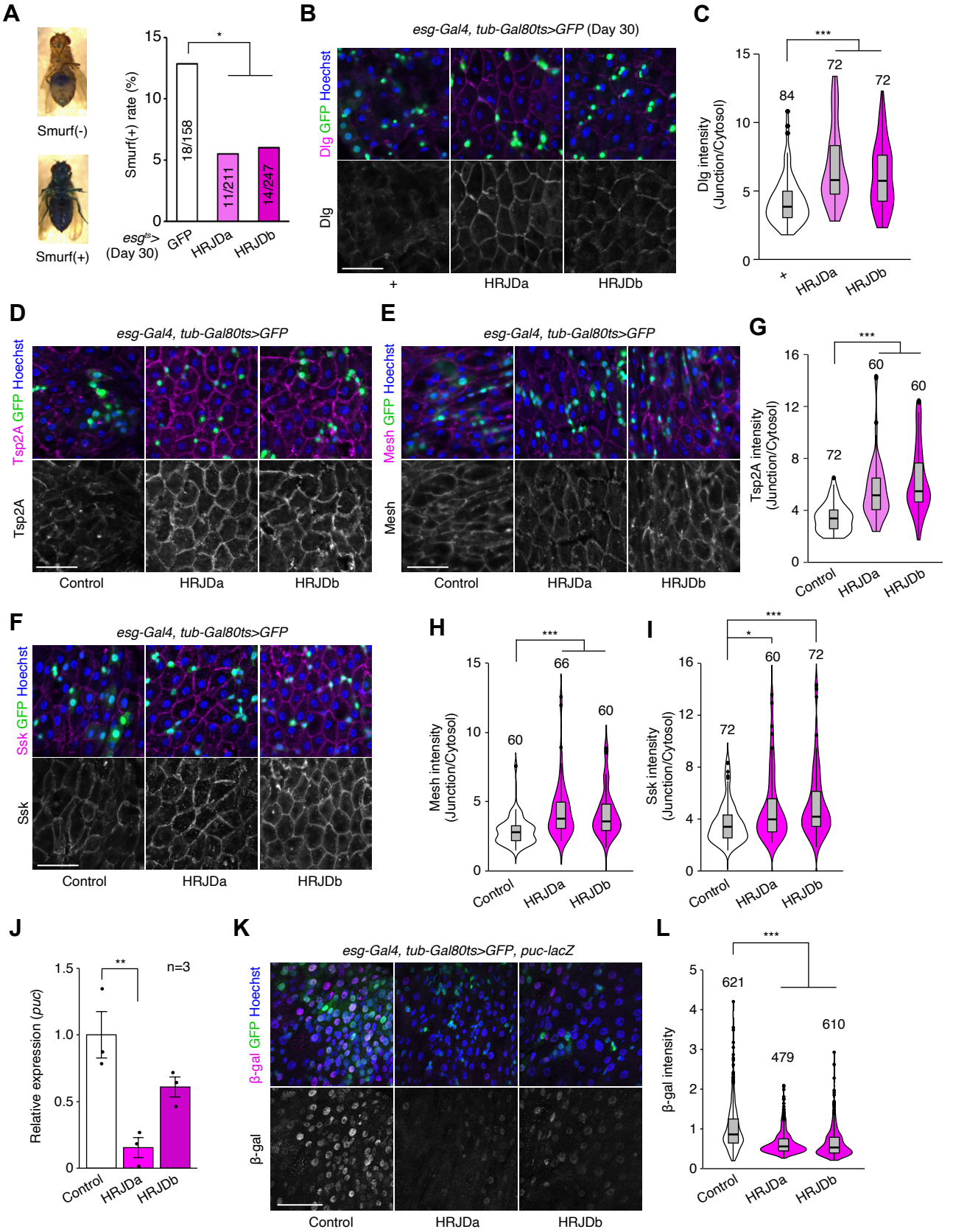
A
Smurf(-)
Smurf(+)
Smurf(+) rate (%)
18/158
11/211
14/247
esg^ts> (Day 30)
GFP
HRJDa
HRJDb
B
esg-Gal4, tub-Gal80ts>GFP (Day 30)
Dlg GFP Hoechst
Dlg
+
HRJDa
HRJDb
C
Dlg intensity (Junction/Cytosol)
84
72
72
D
esg-Gal4, tub-Gal80ts>GFP
Tsp2A GFP Hoechst
Tsp2A
Control
HRJDa
HRJDb
E
esg-Gal4, tub-Gal80ts>GFP
Mesh GFP Hoechst
Mesh
Control
HRJDa
HRJDb
G
Tsp2A intensity (Junction/Cytosol)
72
60
60
F
esg-Gal4, tub-Gal80ts>GFP
Ssk GFP Hoechst
Ssk
Control
HRJDa
HRJDb
H
Mesh intensity (Junction/Cytosol)
60
66
60
I
Ssk intensity (Junction/Cytosol)
72
60
72
J
Relative expression (puc)
n=3
Control
HRJDa
HRJDb
K
esg-Gal4, tub-Gal80ts>GFP, puc-lacZ
β-gal GFP Hoechst
β-gal
Control
HRJDa
HRJDb
L
β-gal intensity
621
479
610

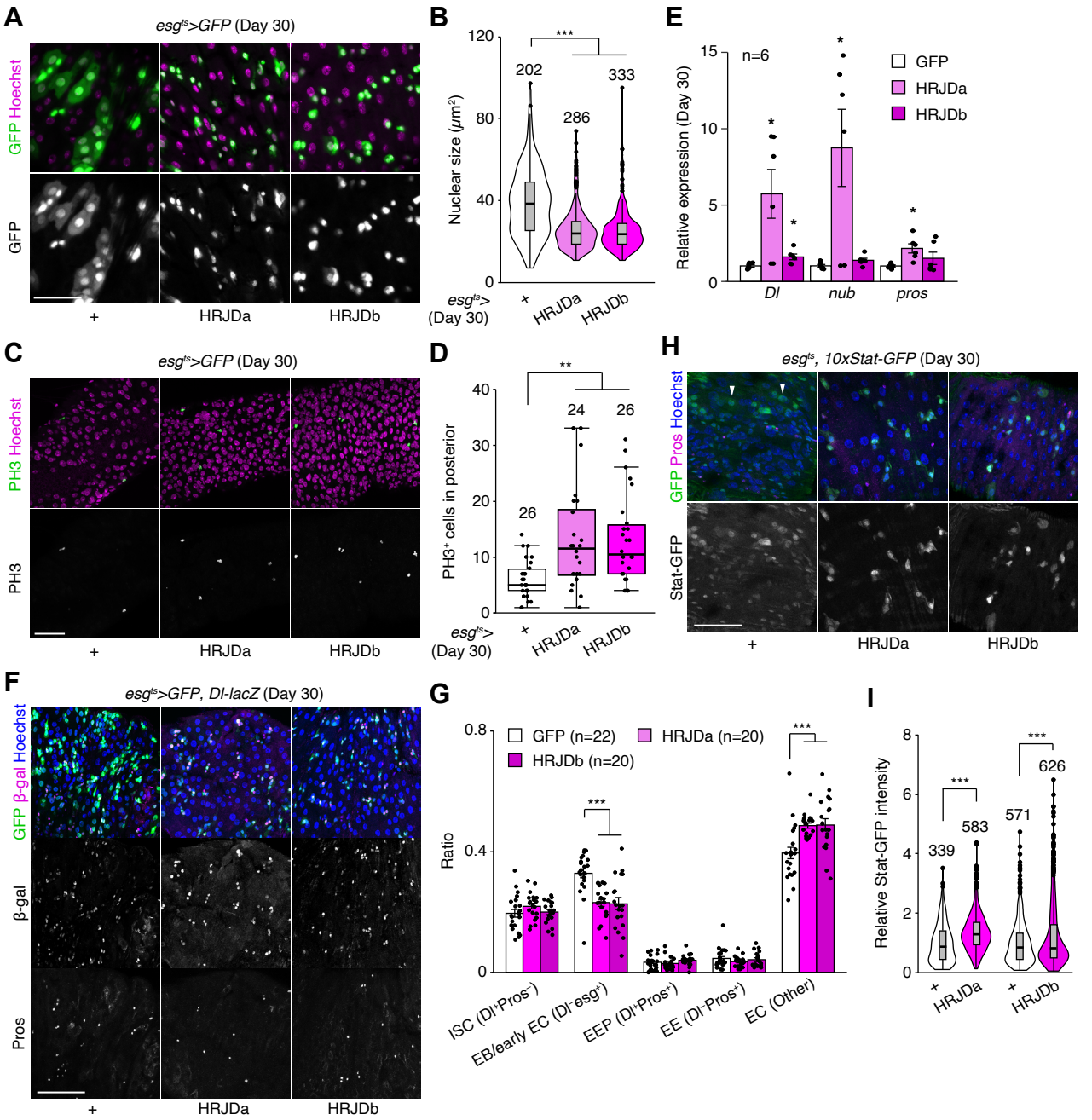
A
esgts>GFP (Day 30)
GFP Hoechst
GFP
+
HRJDa
HRJDb
B
Nuclear size (μm2)
esgts> (Day 30)
202
286
333
***
C
esgts>GFP (Day 30)
PH3 Hoechst
PH3
D
PH3+ cells in posterior
26
24
26
**
E
Relative expression (Day 30)
n=6
GFP
HRJDa
HRJDb
Dl
nub
pros
H
esgts, 10xStat-GFP (Day 30)
GFP Pros Hoechst
Stat-GFP
F
esgts>GFP, Dl-lacZ (Day 30)
GFP β-gal Hoechst
β-gal
Pros
G
Ratio
GFP (n=22)
HRJDa (n=20)
HRJDb (n=20)
ISC (Dl+Pros-)
EB/early EC (Dl-esg+)
EEP (Dl+Pros+)
EE (Dl-Pros+)
EC (Other)
I
Relative Stat-GFP intensity
339
583
571
626

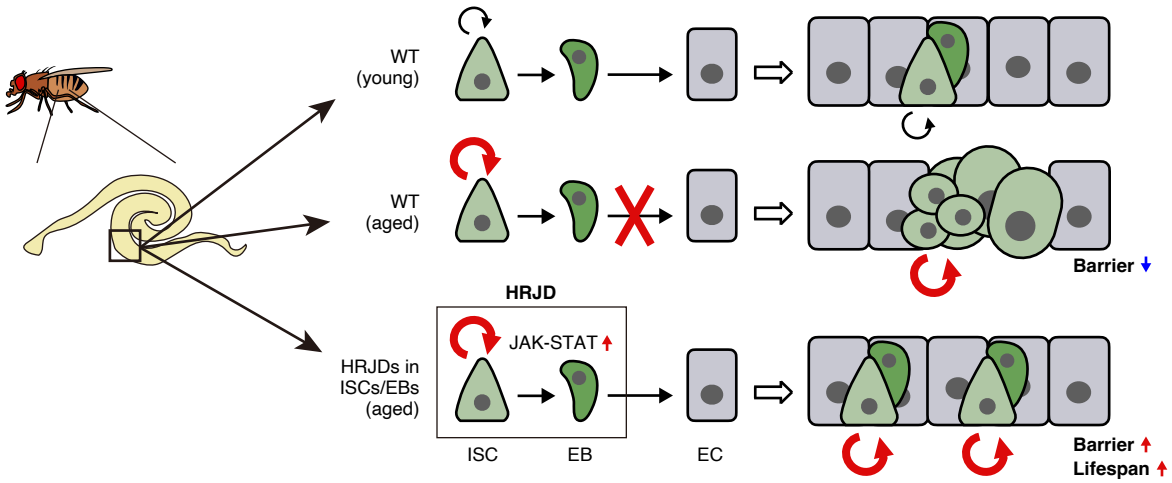
WT
(young)
WT
(aged)
HRJDs in
ISCs/EBs
(aged)
HRJD
JAK-STAT
ISC
EB
EC
Barrier
Barrier
Lifespan